Max-Planck-Institut für Meteorologie

REPORT No. 203

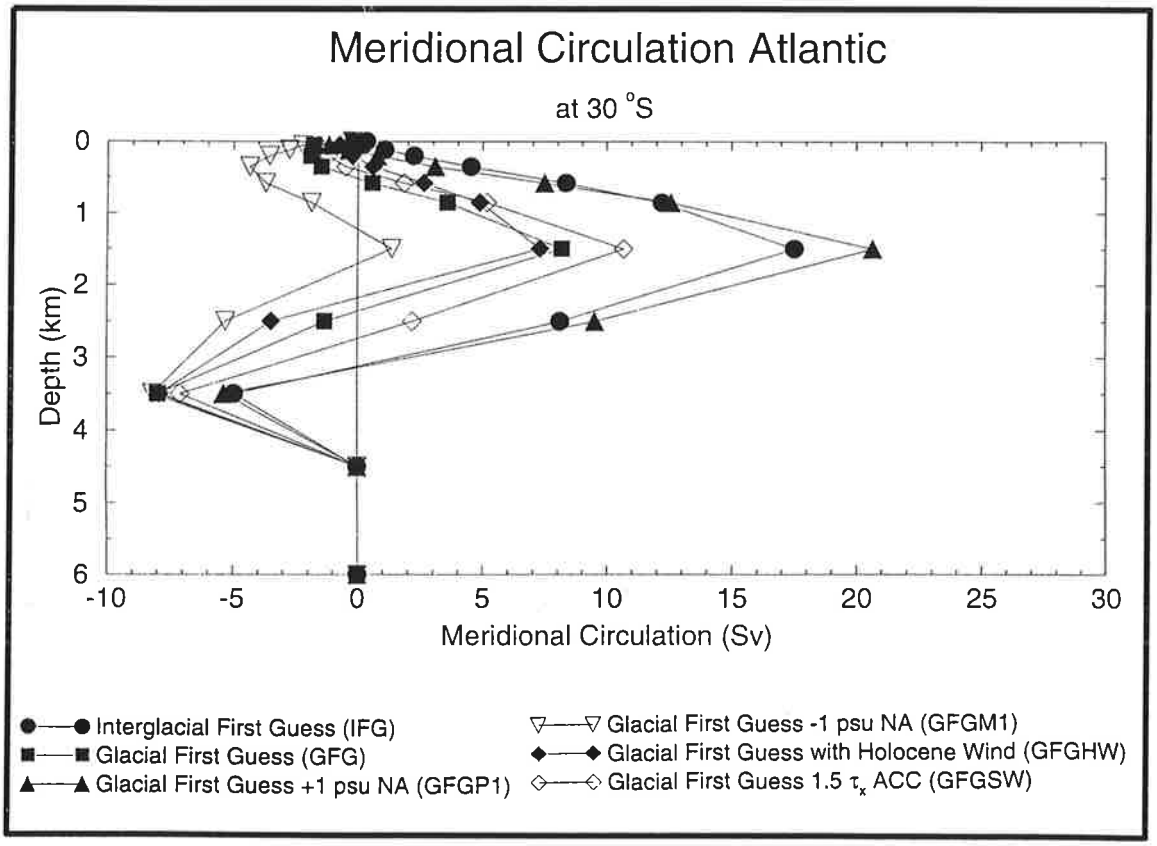

ON THE SENSITIVITY OF AN OCEAN GENERAL CIRCULATION MODEL TO GLACIAL BOUNDARY CONDITIONS

by

Arne M. E. Winguth • Ernst Maier-Reimer
Uwe Mikolajewicz • Jean-Claude Duplessy

HAMBURG, July 1996

AUTHORS:

Arne M. E. Winguth
Ernst Maier-Reimer
Uwe Mikolajewicz

Max-Planck-Institut
für Meteorologie

Jean-Claude Duplessy

Centre des Faibles Radioactivites
Laboratoire mixte CNRS-CEA
91198 Gif sur Yvette cedex
France

MAX-PLANCK-INSTITUT
FÜR METEOROLOGIE
BUNDESSTRASSE 55
D - 20146 HAMBURG
GERMANY

Tel.: +49-(0)40-4 11 73-0
Telefax: +49-(0)40-4 11 73-298
E-Mail: <name> @ dkrz.de

ISSN 0937-1060

On the sensitivity of an ocean general circulation model to glacial boundary conditions

A. M. E. Winguth, E. Maier-Reimer, and U. Mikolajewicz
Max-Planck-Institut für Meteorologie, Hamburg, Germany

J.-C. Duplessy
Centre des Faibles Radioactivites Laboratoire mixte CNRS-CEA, Gif sur Yvette, France

July 7, 1996

ISSN 0937-1060

Abstract. Several studies in the last two decades measuring stable isotope ratios $\delta^{13}C$ from foraminifera shells pointed out that during the last glacial maximum (LGM) the Atlantic thermohaline circulation was significantly different from the present day circulation, indicating a shallower and reduced North Atlantic Deep Water (NADW), while the compensating Antarctic Bottom Water (AABW) penetrated further northward. Here, we show a 3 D OGCM response to glacial wind stress and air temperature derived from an atmospheric GCM and salinity reconstructions adapted from $\delta^{18}O$ measurements in foraminifera shells. The OGCM includes a simplified biogeochemical cycle and reproduces the main features of the past $\delta^{13}C$ distribution with a reduction of the Atlantic 'conveyor belt' by about the half at 30 °S. Sensitivity experiments with respect to possible errors in the reconstructed salinity boundary fields show circulation patterns in the Atlantic ranging from an even stronger than the present day one to a nearly shut down of the 'conveyor belt' circulation. Additionally, a sensitivity experiment with respect to uncertainties of the wind field in order of the glacial-interglacial amplitude shows that Atlantic overturning circulation is not severely affected.

1. Introduction

Geological proxies indicate that during glacial periods the climate was significantly different from todays interglacial state (for an overview see e.g. *Crowley and North* [1991]). It is widely accepted that changes of the Atlantic 'great conveyor belt' [*Broecker*, 1987] which transports warm water north and cold dense water south are linked considerably with these climate variations.

A common geological tool to reconstruct the ocean circulation during the last glacial maximum (LGM) 21,000 years ago is the distribution of the $\delta^{13}C$ ratio of calcareous shells of benthic foraminifera sampled through marine sediment cores [e.g., *Curry and Lohmann*, 1983; *Boyle and Keigwin*, 1987; *Duplessy et al.*, 1988; *Sarnthein et al.*, 1994]. The vertical gradients of the $\delta^{13}C$ ratio in the ocean are strongly attributed to a biological pumping mechanism, the "soft tissue pump" [*Volk and Hoffert*, 1985]. At the surface, ^{12}C is preferably incorporated in the soft tissue relative to ^{13}C yielding a $\delta^{13}C$ ratio in the organic material which is about -20 ‰ lower than in the surrounding water. The soft tissue provided by primary production at the sea surface is transferred to the deep sea where most of the parts are remineralized. Thus the surface ocean has relatively high $\delta^{13}C$ ratios while the deep sea shows low ratios. The circulation, however, effects the nutrient and $\delta^{13}C$ distribution in a complex way and changes in the circulation also cause changes in the biological pump as well as changes in the $\delta^{13}C$ distribution.

The geological studies supported theories of different modes of the Atlantic circulation [*Stommel*, 1961; *Rooth*, 1982] due to significant fluctuations of high latitude boundary conditions (e.g., wind, air temperature and freshwater pattern) in the past. Several experiments with three-dimensional [e.g., *Maier-Reimer and Mikolajewicz*, 1989; *England*, 1993; *Rahmstorf*, 1994; *Tziperman et al.*, 1994; *Seidov et al.*, 1996; *Schiller et al.*, manuscript submitted] and two-dimensional [e.g., *Stocker et al.*, 1992; *Fichefet et al.*, 1994] ocean circulation models suggested a high sensitivity of the Atlantic circulation

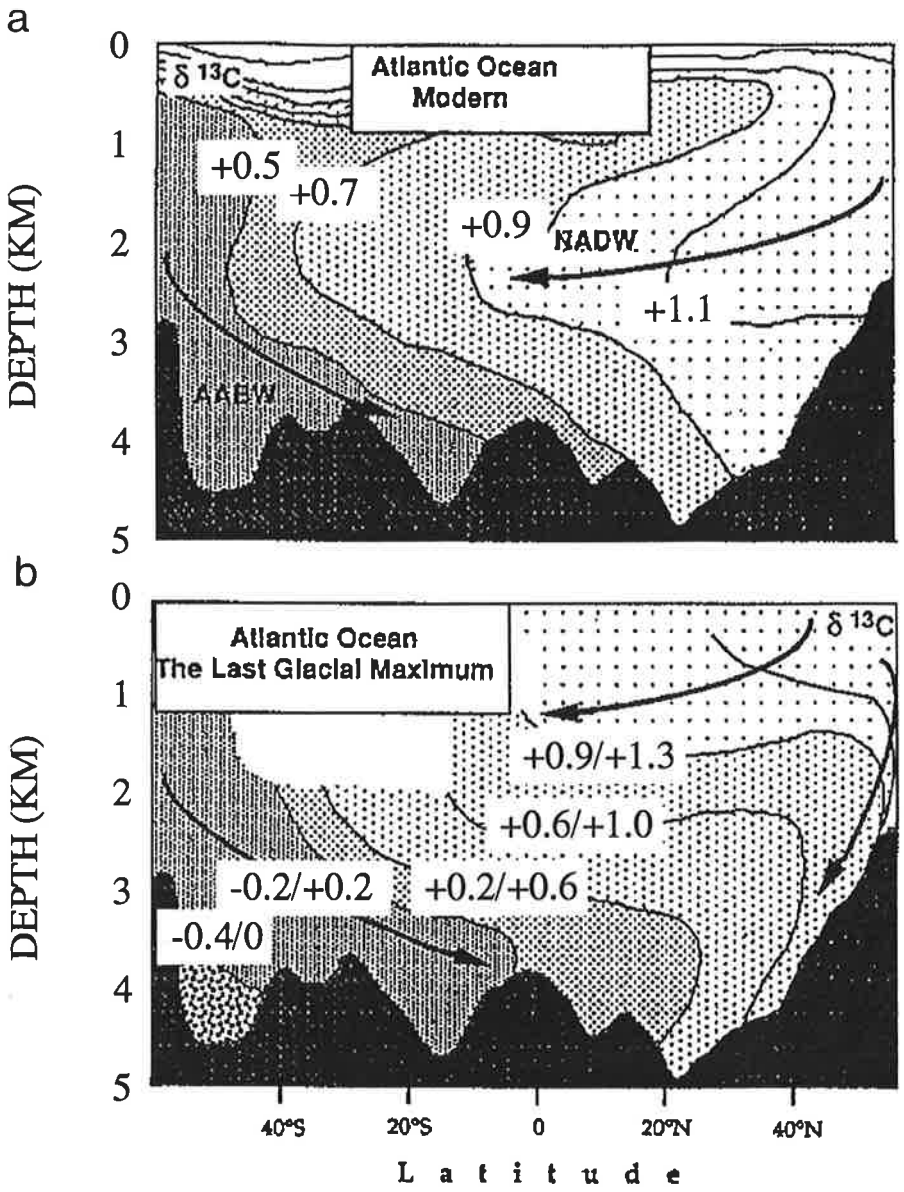

Fig. 1. Reconstruction of the changes in $\delta^{13}C$ across the Atlantic Ocean: (a) for the modern interglacial period (adapted from *Kroopnick* [1984]), and (b) for the LGM (adapted from the foraminifera shell $\delta^{13}C$ distribution of *Duplessy et al.* [1988]). Numbers behind the slash refer to values after subtracting the global mean glacial-interglacial shift of -0.4 ‰ (redrawn after *Labeyrie et al.* [1992]).

due to perturbation in the surface buoyancy forcing in the polar regions. These authors showed that the strength of the 'conveyor' significantly depends on the density contrast between high latitudes of the northern and southern hemispheres. *Hughes and Weaver* [1993] used an OGCM to examine the role of model geometry and surface buoyancy and windstress forcing in the asymmetry of the global thermohaline circulation. Their model results showed that multiple 'conveyor'-type equilibria with different strengths of the North Atlantic overturning are very sensitive to the bathymetry and to prescribed temperature and salinity forcing. With modern forcing and topography OGCMs are capable of exhibiting at least three different types of equilibria in the Atlantic [*Mikolajewicz et al.*, 1993]: The first mode ('conveyor on') corresponds to the present day circulation with a strong North Atlantic Deep Water (NADW) formation (Figure 1a). The second mode ('conveyor reduced') with a reduced NADW flow and a stronger influence of Antarctic Bottom Water (AABW) characterizes the situation during the LGM (Figure 1b) as shown by *Heinze et al.* [1991] with a carbon cycle model (which simulates a $\delta^{13}C$ distribution similar to Figure 1b). The third mode ('inverse conveyor') has similarities to the recent Pacific circulation.

In contrast to the Atlantic Ocean, climate fluctuations of the past 21,000 years in deeper Pacific Ocean seem to be much weaker. With a presumably more ventilated upper Pacific [*Boyle*, 1992; *Keigwin et al.*, 1992], the LGM circulation field of the two oceans appeared more symmetrically, while todays circulation has a more antisymmetric structure [*Broecker*, 1993]. However, the geological $\delta^{13}C$ reconstructions cannot be applied to large areas of the deep northern Pacific, or Antarctic Circumpolar Current, which are almost free of calcareous sediment.

Several geochemical box models [e.g., *Knox Ennever and McElroy*, 1985; *Toggweiler and Sarmiento*, 1985; *Wenk and Siegenthaler*, 1985; *Broecker and Peng*, 1986; *Keir*, 1988; *Michel et al.*, 1995] have been developed to explain the LGM $\delta^{13}C$ distribution and atmospheric CO_2 level which was reduced by about 30% compared with the

preindustrial value of about 280 ppm [*Barnola et al.*, 1987]. These models also generally support the geological assumptions of a reduced Atlantic 'conveyor' during the last glacial maximum.

One direct approach to reproduce the glacial ocean circulation has been examined with the Hamburg large scale geostrophic (LSG) oceanic general circulation model (OGCM) forced with sea surface temperatures from the CLIMAP Project Members [1981] and wind stress and freshwater flux derived from the ice age response of an atmospheric GCM [*Lautenschlager et al.*, 1992]. The glacial changes in the physical ocean appeared to have the correct sign, but they were too large. The authors concluded that insufficient data for surface boundary conditions might have caused these deviations.

Fichefet et al. [1994] evaluated a reduced Atlantic 'conveyor' of about 40% with a zonally averaged ocean circulation model. Their model was forced with the same LGM boundary conditions for wind stress and temperature as in the study of *Lautenschlager et al.* [1992] and prescribed salinity deduced from reconstructions derived from δ^{18}O analysis in foraminifera shells [*Duplessy et al.*, 1991]. The surface δ^{18}O is obtained by computing the oxygen isotopic fractionation at temperature relevant for the growth of the shells. Salinity may then be calculated using a linear [*Duplessy et al.*, 1991] or nonlinear relation [*Schaefer-Naeth*, 1994] between surface water $\delta^{18}O_{SMOW}$ (Standard Mean Ocean Water) and salinity observed for modern North Atlantic Ocean GEOSECS data [*Östlund et al.*, 1987]. The slope between the two tracers is varying for surface water between 0.1 (for tropical regions) to 0.6 (for high latitudes) [*Craig and Gordon*, 1965] due to the regional fresh water dilution into sea water. In polar regions the waters have a relatively wide range of salinities influenced by freezing processes even though they have virtually the same $\delta^{18}O_{SMOW}$ [*Zahn and Mix*, 1991]. More recently, *Mikolajewicz* [1996] pointed out that errors in the reconstruction of salinity from δ^{18}O in sea water could be larger than 1 psu during a meltwater input from the glacial ice

sheets, which has a different isotopic composition than the surrounding sea water. Thus the slopes between surface water $\delta^{18}O_{SMOW}$ and salinity might have changed during glacial times where sea ice freezing had been significantly increased.

Another major uncertainty comes from the errors derived from the sea surface temperature reconstructions. A typical $\pm$ 1 °C uncertainty introduces an about $\pm$ 0.5 psu error on salinity. Other errors may arise from uncertainties from the foraminiferal $\delta^{18}O$ measurements themselves, and from the sparse coverage of $\delta^{18}O$ cores for most parts of the ocean.

A straightforward technique to reconstruct the steady LGM ocean circulation would be the direct assimilation of $\delta^{13}C$ ratios from marine sediment cores into an ocean model. *Heinze and Hasselmann* [1993] used a linear model optimally fitted to ice and marine sediment core records for the last 120,000 yr to estimate the carbon cycle parameter changes that could have caused the observed reduction of atmospheric pCO_2 during the last glaciation. *Le Grand and Wunsch* [1995] applied a coarse resolution inverse model to simulate the LGM circulation of the North Atlantic. The latter authors conclude that the geological assumption of a reduced 'conveyor' satisfies the $\delta^{13}C$ data constraint as well as a circulation pattern similar to the modern interglacial one. The latter is supported by a more recent analysis of radioactive tracers in marine sediment cores [*Yu et al.*, 1996]. However, *Le Grand and Wunsch* neglect changes in the biological pump which also affect the $\delta^{13}C$ distribution of the past ocean deep water.

Assimilation of $\delta^{13}C$ data by using the adjoint technique [e.g., *Le Dimet and Talagrand*, 1986] into a global OGCM including marine biology can evaluate an optimal circulation pattern and surface boundary conditions consistent with the dynamics of the model and minimal distance between the geological data and model counterparts. This method has the disadvantage that it is relatively expensive in computational costs and that the iteration for optimization may converge in a secondary minimum. Thus it is necessary to construct a first guess as a starting point for the assimilation which is close

enough to the geological data base.

In this study we present experiments with an OGCM [*Maier-Reimer et al.*, 1993] including a simplified biological cycle, run with prescribed LGM boundary conditions to provide a first guess for data assimilation. In addition we show the sensitivity of the thermohaline circulation due to possible errors of the surface salinity pattern reconstructed from $\delta^{18}O$ distribution in foraminifera shells and due to changes of the wind fields.

2. Model Description

2.1 Ocean General Circulation Model

The Hamburg large scale geostrophic model (LSG), described in detail in *Maier-Reimer et al.* [1993], is based on the conservation laws for heat, salt, and momentum (the latter in linearized form), the full equations of state, and the hydrostatic approximation. Gravity waves are suppressed by the implicit integration scheme, permitting a free sea surface elevation. Additionally the Boussinesq approximation is applied and vertical friction is neglected. The circulation is divided into a barotropic component, consistent of the vertical integrated circulation field and the surface elevation, and baroclinic components, which describe the residual current after subtraction of the barotropic mode. The motion outside the equator is essentially in geostrophic balance with frictional effects. Prognostic variables are sea ice, temperature, and salinity, to which the velocities and surface elevation on the time scale of interest adjust almost immediately. Three prognostic geochemical tracers, phosphate (PO_4), particulate organic carbon (POC), and oxygen (O_2) are included. This represents a chemically consistent reduction of the full HAMOCC3 [*Maier-Reimer*, 1993] phosphate cycle model. The model runs on a global 72 x 72 E grid [*Arakawa and Lamb*, 1977](approximate 3.5^o x 3.5^o horizontal resolution), 11 vertical layers with realistic bathymetry, and has a time step of one

month in order to resolve the seasonal cycle. The temperature and salinity in the surface layer were computed by a Newtonian coupling to prescribed air temperatures and salinities. A coupling coefficient of 40 W m^{-2} s^{-1} for temperature and 1.5 x 10^{-5} m s^{-1} for salinity yields (for a 50-m thick top layer) a time constant for both properties of approximately 40 days.

2.2 Biological Model

For this study the Hamburg LSG model is extended by a simplified biological model which is used instead of the 3 D carbon cycle model [*Maier-Reimer*, 1993] in order to reduce computational costs and complexity. The idea of the model applied here is to simulate only the soft tissue pump [*Volk and Hoffert*, 1985] which can explain more than 80% of the vertical carbon gradients in the ocean [*Maier-Reimer et al.*, 1987].

Phosphate, chosen as a limiting nutrient tracer, is consumed by primary production in the surface and released in the deep sea by remineralization. The model assumes for these processes a constant Redfield ratio [*Takahashi et al.*, 1985; *Broecker and Peng*, 1992]

$$P : N : C : \Delta O_2 = 1 : 16 : 127 : -172 \qquad (1)$$

Export production (NP), the part of primary production transported into deeper levels [*Eppley and Peterson*, 1979], is parameterized by the Michaelis Menten kinetic formula according to *Dugdale* [1967]. The formula (see *Maier-Reimer* [1993], page 653) depends on light intensity, phosphate, potential temperature ϑ and convective mixing. Hence, the three prognostic geochemical tracers change in the surface under consideration of

partial remineralization of POC (B):

$$\begin{aligned} [POC] &= [POC] + NP - B \\ [PO_4] &= [PO_4] - (NP - B)\,/\,\mathrm{RC} \\ [O_2] &= [O_2] + \mathrm{ROC} \cdot (NP - B) \end{aligned}$$

where ROC and RC denotes the Redfield ratio $\Delta O_2 : C$ and $P : C$. The change of the oxygen concentration in the surface layer is only a secondary process because we assume an almost 100% O_2 saturation due to the gas exchange with the atmosphere. The gas exchange is modeled according to Henry's law under consideration of a solubility from *Weiss* [1970]. Much of the soft tissue sinks downward in large aggregates - fecal pellets - in a relatively short time compared to the advection [*Honjo*, 1982]. Below the euphotic zone which is represented by the top 50-m-thick layer of the model, the downward flux of soft tissue is modeled according to *Berger et al.* [1987] proportionally to $z^{-0.8}$, where z denotes the depth. With increasing depth, concentration of phosphate increases while O_2 concentration decreases through the remineralization of POC. The remineralization is limited to regions with sufficient oxygen. Unremineralized POC is preserved and advected by the circulation. According to measurements from the GEOSECS expediton [*Kroopnick*, 1985; *Östlund et al.*, 1987], δ^{13}C for dissolved ΣCO_2 is in most parts of the deep ocean well correlated to phosphate. Neglecting the thermodynamic effect (including the influence of gasexchange with atmospheric CO_2) for the deep sea we use a linear relationship from *Broecker and Maier-Reimer* [1992] to calculate the δ^{13}C ratio diagnostically from the phosphate concentration:

$$\delta^{13}\mathrm{C} = 2.9 - 1.1\, PO_4 + c \qquad (2)$$

based on a mean concentration of 2200 μmol kg^{-1} for ΣCO_2 and 2.2 μmol kg^{-1} for PO_4. c is an offset constant to adjust the modeled δ^{13}C distribution to the δ^{13}C GEOSECS data of the deep Atlantic [*Kroopnick*, 1985] and is taken to be -0.25 $^{o}/_{oo}$.

Table 1. Overview of Sensitivity Experiments

Experiment	Boundary Condition		
	Temperature	Salinity	Wind Stress
IFG	COADS	LEVITUS	ECHAM3/T42 (Holocene)
GFG	ECHAM3/T42 (LGM)	LEVITUS +DUPLESSY NA: -0.50 psu SA: +0.75 psu	ECHAM3/T42 (LGM)
GFGP1	ECHAM3/T42 (LGM)	LEVITUS +DUPLESSY NA: +0.50 psu SA: +0.75 psu	ECHAM3/T42 (LGM)
GFGM1	ECHAM3/T42 (LGM)	LEVITUS +DUPLESSY NA: -1.50 psu SA: +0.75 psu	ECHAM3/T42 (LGM)
GFGHW	ECHAM3/T42 (LGM)	LEVITUS +DUPLESSY NA: -0.50 psu SA: +0.75 psu	ECHAM3/T42 (Holocene)
GFGSW	ECHAM3/T42 (LGM)	LEVITUS +DUPLESSY NA: -0.50 psu SA: +0.75 psu	ECHAM3/T42 (LGM) ACC: 1.5 τ_x

5 sensitivity experiments with different prescribed boundary conditions have been carried out: interglacial first guess (IFG) is taken as reference run with present-day boundary conditions, glacial first guess (GFG) with LGM boundary conditions, and two experiments (GFGP1 and GFGM1) with the same LGM boundary conditions as in the GFG experiment and additional salinity anomalies in the North Atlantic. In the GFGHW experiment Holocene wind stress forcing was used and in the GFGSW experiment LGM wind stress was intensified in the zonal component by a factor of 1.5 (including a smooth transition) in the region of the Southern Ocean. In the GFGHW and GFGHW experiment the same thermohaline boundary conditions were used as in the GFG experiment. NA denotes the North Atlantic north of 50°N and SA the South Atlantic south of 50°S (including a linear transition between 40°and 50°). ACC denotes here the region between 67.5 °S and 40 °S.

3. Experiments

Long term variations of the ocean circulation are influenced by changes of sea surface boundary conditions (temperature, salinity, and momentum fluxes) as well as changes in bottom topography due to plate tectonics, water volume changes, and isostatic rebounds. Five sensitivity experiments with different interglacial and glacial boundary conditions were carried out (listed in Table 1):

Experiment IFG corresponds to the interglacial reference run or interglacial first guess for data assimilation. The model was forced with present day boundary conditions. The Bering Street is open.

Experiment GFG , the glacial first guess, simulates the glacial circulation under LGM boundary conditions. Here, the Bering Street was closed and topography otherwise was unchanged. However, previous experiments with the Hamburg LSG model showed that the closed Bering Street did not cause significant changes in the circulation pattern.

Experiments GFGP1 (GFG plus 1 psu) and GFGM1 (GFG minus 1 psu) estimate the changes of circulation due to possible errors in the LGM salinity pattern reconstructed from the $\delta^{18}O$ in the planctonic foraminifera shells. The model was forced with the same boundary conditions as in GFG and an additional salinity anomaly of +1 psu respectively -1 psu in the Atlantic north of 50 °N.

Experiments GFGHW (GFG Holocene wind) and GFGSW (GFG strong Westwind), finally, investigate the sensitivity of thermohaline circulation to uncertainties in the LGM wind fields. The model was driven in both experiments with the same thermohaline boundary conditions as in the GFG experiment. Experiment GFGHW used Holocene wind as in the IFG experiment and GFGSW used LGM wind stress intensified in the zonal component by a factor of 1.5 in the region of the Southern Ocean.

All experiments were integrated (of order 4000 years and more) with the forcing fields until a steady state of the circulation was achieved.

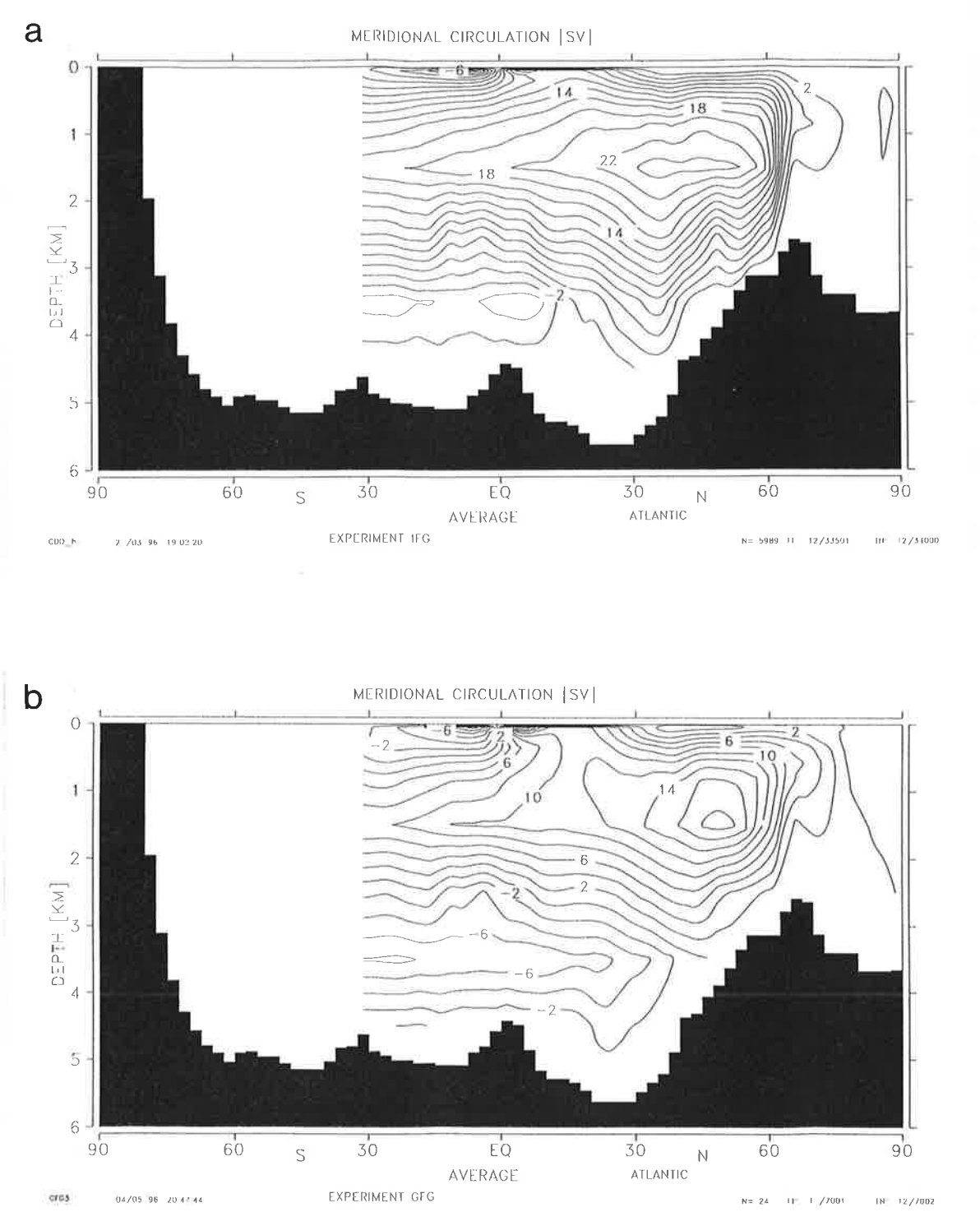

Fig. 2. Annual mean of zonally averaged Atlanic merdional circulation: (a) OGCM response to present-day boundary conditions (IFG experiment), and (b) OGCM response to LGM boundary conditions (GFG experiment). Contour interval: 2 Sv (1 Sv = 10^6 m $^3s^{-1}$).

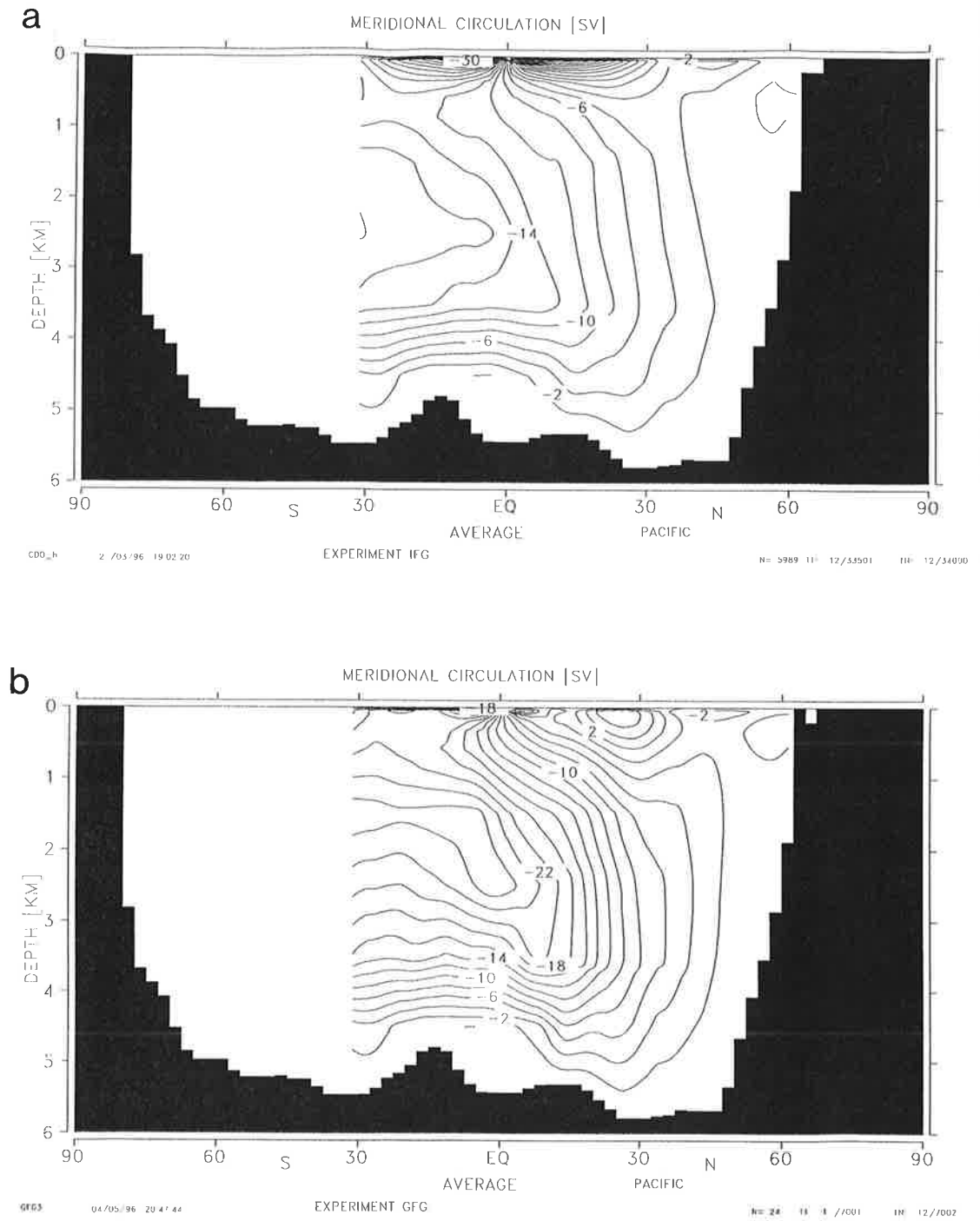

Fig. 3. Annual mean of zonally averaged Pacific merdional circulation: (a) OGCM response to present-day boundary conditions (IFG experiment), and (b) OGCM response to LGM boundary conditions (GFG experiment). Contour interval: 2 Sv (1 Sv = 10^6 m $^3s^{-1}$).

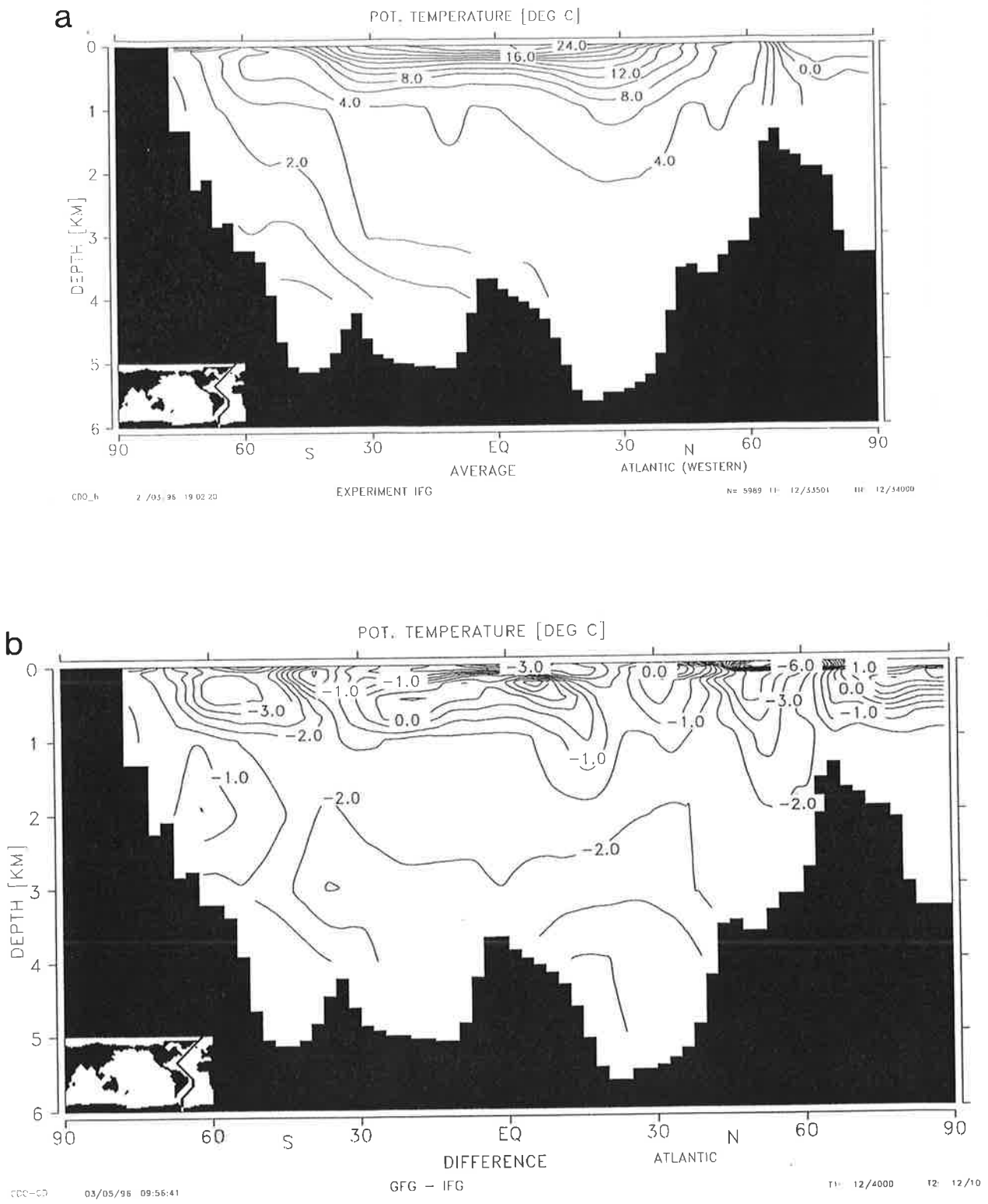

Fig. 4. Annual mean of potential temperature in a section of the western Atlantic: (a) OGCM response to present-day boundary conditions (IFG experiment, contour interval: 1 °C), and (b) LGM minus present-day anomaly (difference between GFG and IFG experiment, contour interval: 0.5 °C).

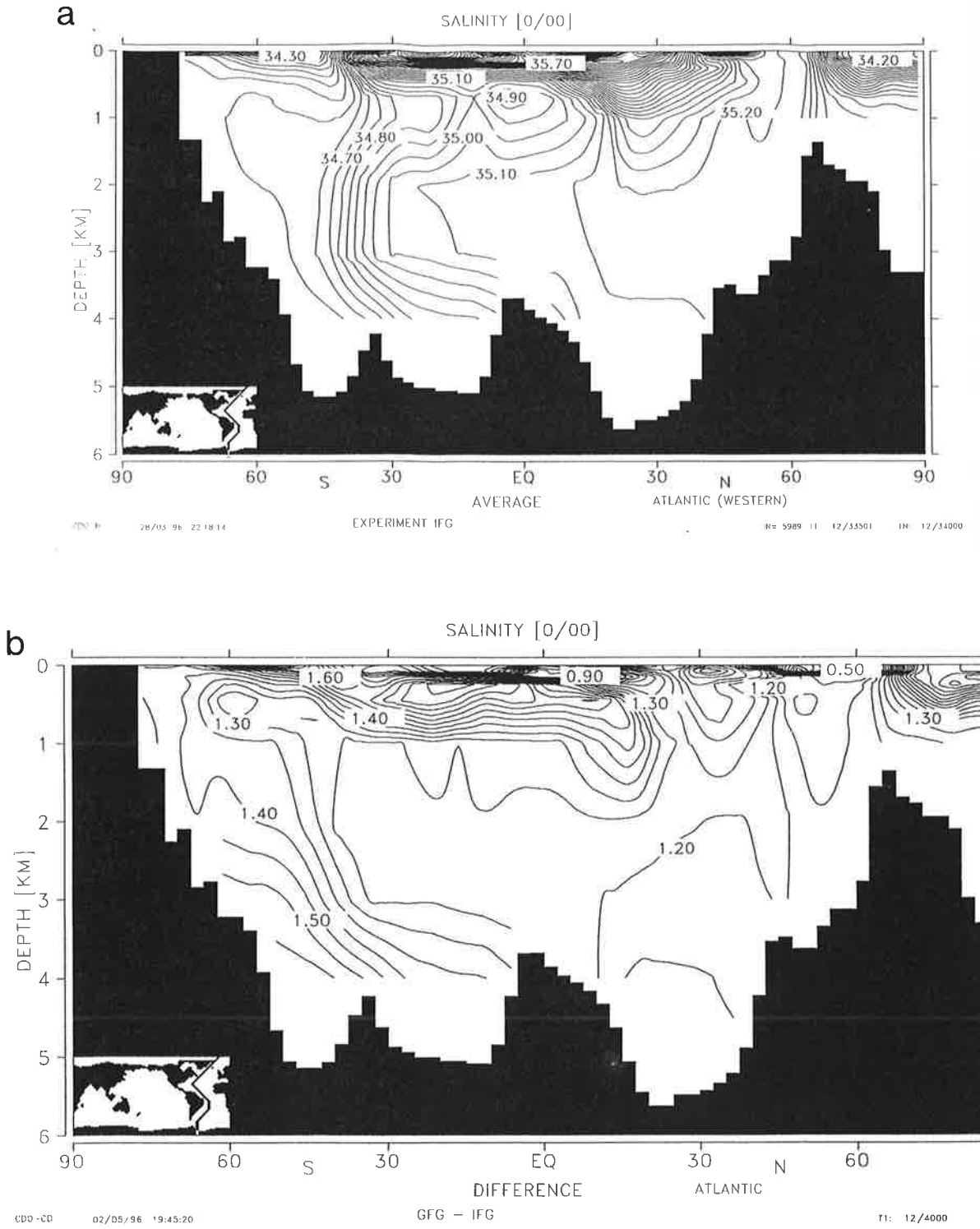

Fig. 5. Annual mean of salinity in a section of the western Atlantic: (a) OGCM response to present-day boundary conditions (IFG experiment, contour interval: 1 psu (1 psu = 1 ‰)), and (b) LGM minus present-day anomaly (difference between GFG and IFG experiment, contour interval: 0.5 psu).

3.1. Experiment IFG - Interglacial First Guess

In the reference experiment, the model was spun up with monthly mean wind stress from the control run of the ECHAM3/T42 atmospheric general circulation model [*Lorenz et al.*, manuscript submitted], monthly mean COADS air temperatures [*Woodruff et al.*, 1987] and annual mean climatological sea surface salinities from *Levitus* [1982]. For phosphate a global mean concentration of about 2.1 μmol l^{-1} [*Conkright et al.*, 1994] is chosen.

The main features of the Atlantic and Pacific steady state circulation (Figure 2a and 3a) are similar to the corresponding fields from the former standard run (ATOS1) in *Maier-Reimer et al.* [1993], which generally reproduce the observed radiocarbon distribution in the world ocean fairly well. The zonally averaged transport of the Atlantic 'conveyor belt' is about 24 Sv at 30 °N, and 18 Sv at 30 °S, about 25% higher than estimations of *Schmitz et al.* [1995]. In the North Atlantic up to 30 °N the model simulates an inflow of cold and dense Antarctic Bottom Water mainly formed in the Ross and Weddell Sea with a net transport of about 5 Sv across 30 °S (slightly lower than the 7 Sv estimations of *Macdonald* [1993]). The deep Pacific circulation shows a deep inflow of about 18 Sv at 30 °S from the Southern Ocean. The strong upwelling of more than 10 Sv into the equatorial region can be seen as an artifact of the zonal integration, which includes the strong upwelling area along the central American west coast.

Figure 4a and 5a show the distribution of potential temperature and salinity along a cross section of the western Atlantic. The model simulates an intensive source of high salinity NADW spreading southward, getting mixed in the Antarctic Circumpolar Current (ACC), and flowing further north into the Indian and Pacific Ocean. However, the model still reproduces in comparison with the data [*Levitus*, 1982] a too salty and

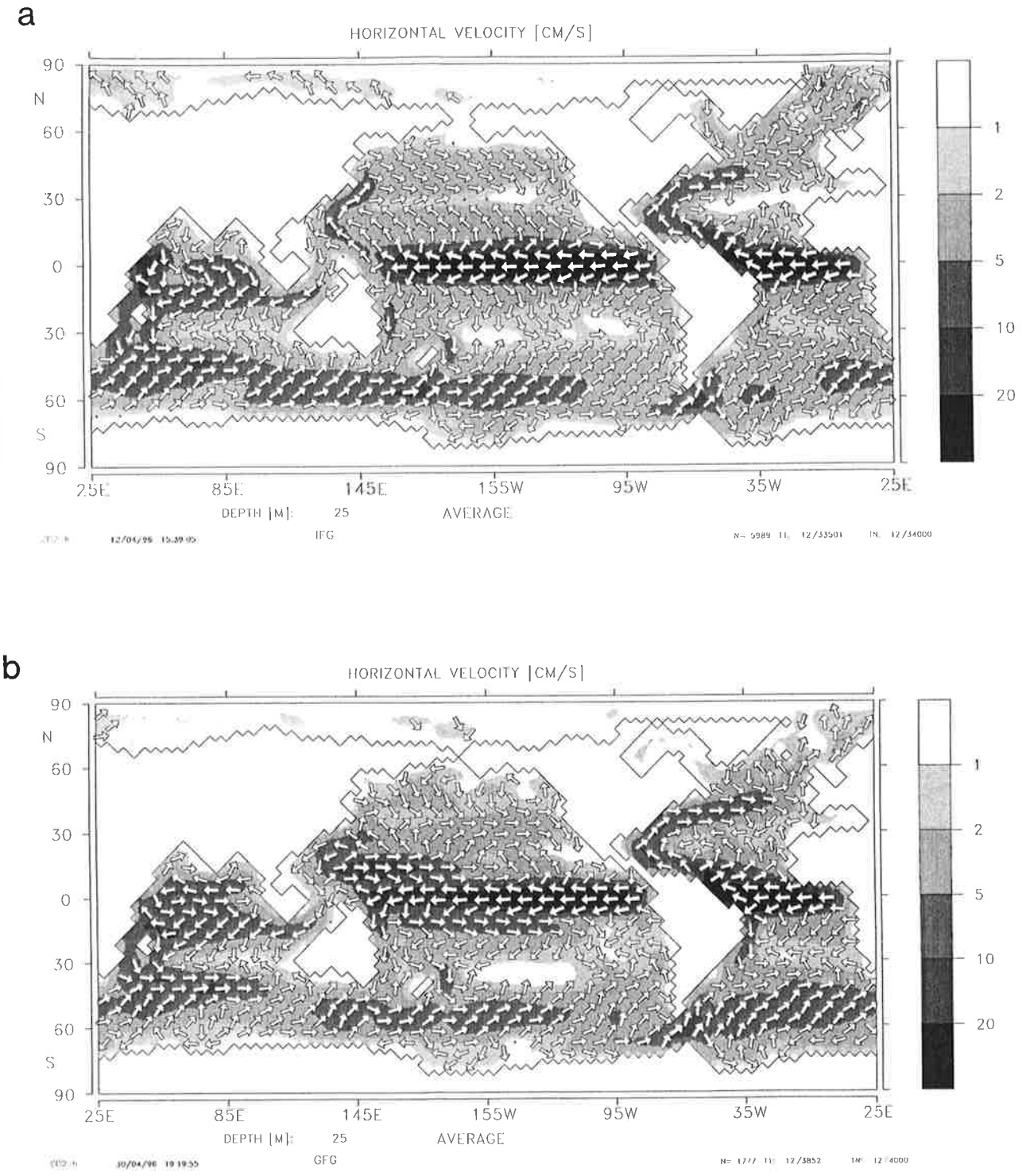

Fig. 6. Annual mean of horizontal velocity in the surface layer: (a) OGCM response to present-day boundary conditions (IFG experiment), and (b) OGCM response to LGM boundary conditions (GFG experiment).

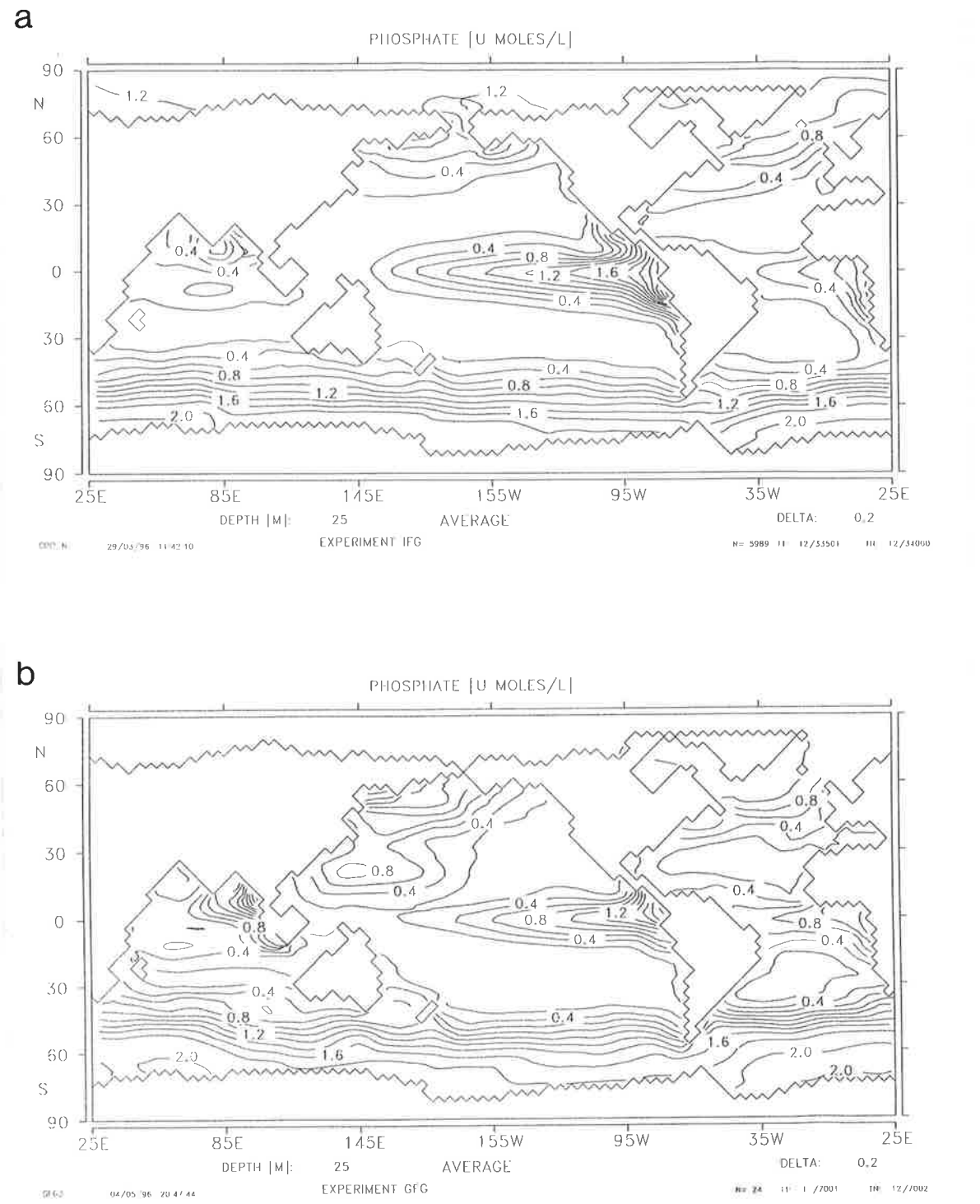

Fig. 7. Annual mean of phosphate concentration in the surface layer: (a) OGCM response to present-day boundary conditions (IFG experiment), and (b) OGCM response to LGM boundary conditions (GFG experiment). Contour interval: 0.2 μmol l^{-1}.

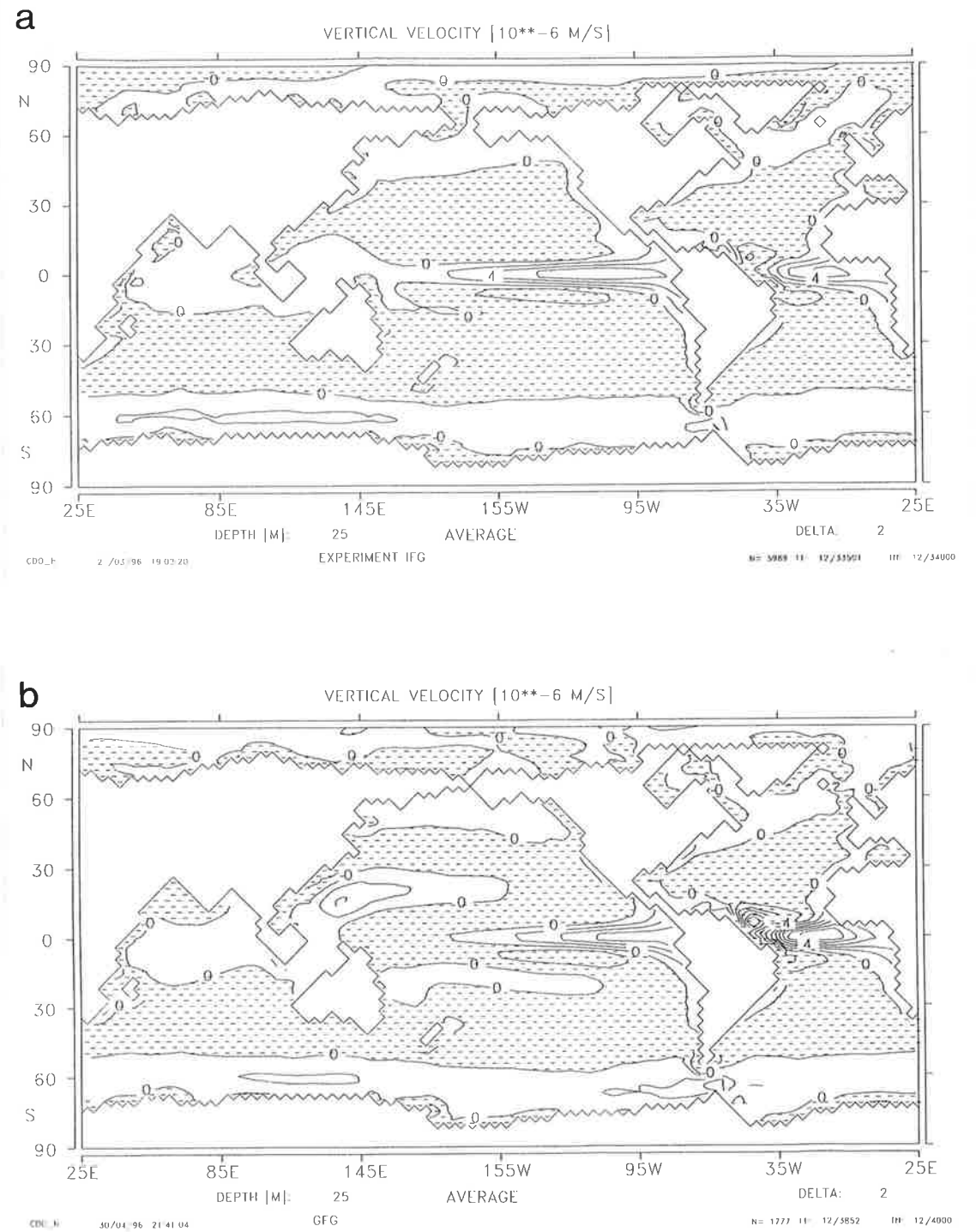

Fig. 8. Annual mean of vertical velocity (between the surface and the second layer): (a) OGCM response to present-day boundary conditions (IFG experiment), and (b) OGCM response to LGM boundary conditions (GFG experiment). The vertical velocity reflects essentially the wind stress divided by the coriolis parameter. Contour interval: 2 x 10^{-6} m s^{-1}.

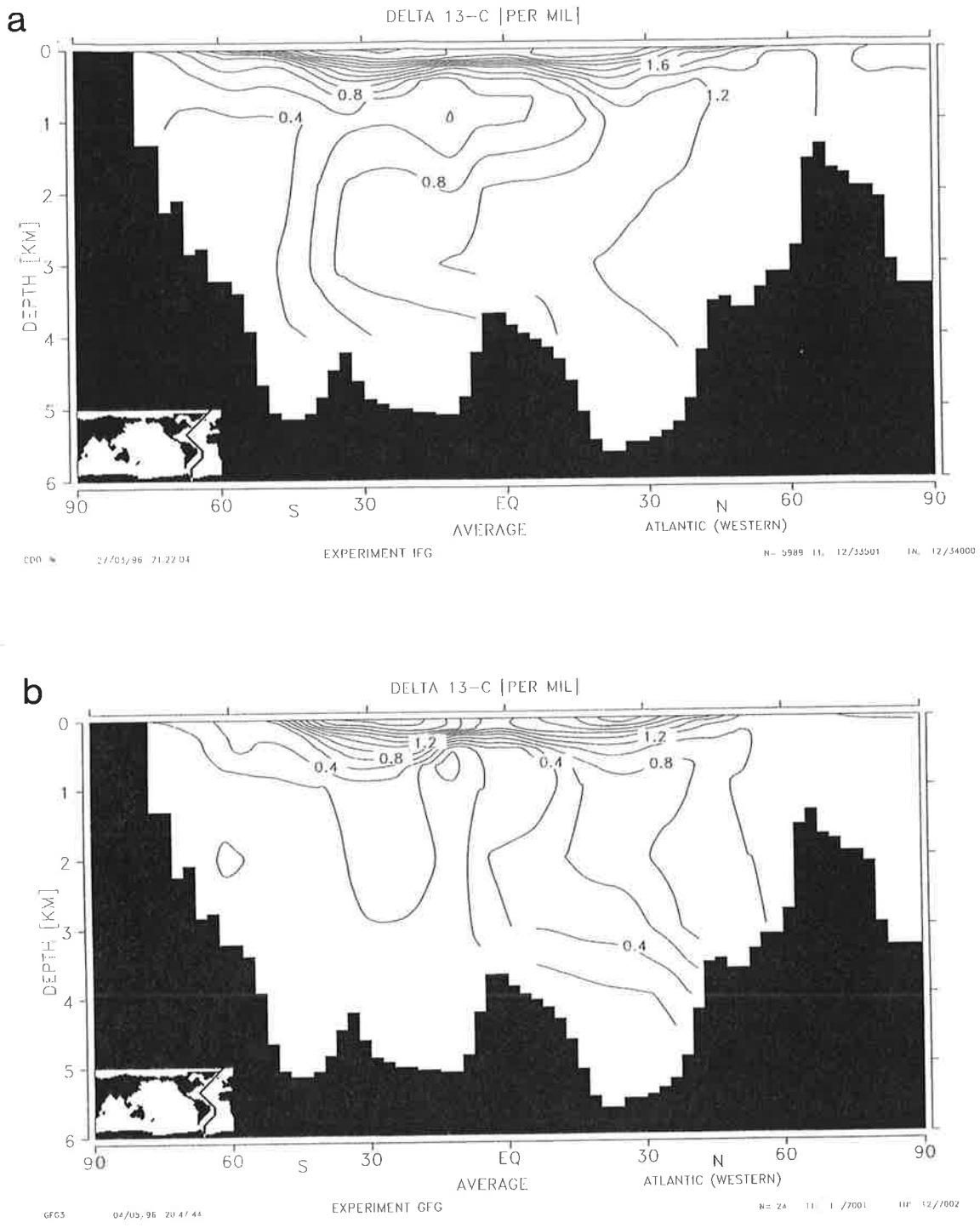

Fig. 9. Annual mean of $\delta^{13}C$ in a section of the eastern Atlantic: (a) OGCM response to present-day boundary conditions (IFG experiment), and (b) anomaly (LGM minus present-day). Contour interval: 0.2 ‰.

warm NADW (the simulated deep Atlantic Ocean (for depth more than 1500m) has an about 0.13 psu too high average salinity of 35.01 psu, and a 0.5 °C too high average potential temperature of 2.6 °C). However, the observed deep ocean temperature and salinity distribution includes past climate variability (e.g., little ice age) and thus may not reflect present surface forcing. The mean salinity of the deep Pacific (34.67 psu) is in concordance with the data, and the potential temperature of the deep Pacific is calculated to be 1.7 °C, which is approximately 0.2 °C too warm in comparison to the corresponding potential temperature calculated from the *Levitus* [1982] data set.

The ACC has a transport of about 115 Sv through the Drake Passage (Figure 6a), about 6% lower than estimations from *Whitworth and Peterson* [1985], while exchange between the Pacific and Indian through the Banda Street is simulated to be about 12 Sv. The feature of the subtropical gyres is reproduced reasonably well. The strength of the Gulf Stream, however, is, due to the coarse resolution of the model, significantly underestimated and too sluggish.

The distribution of phosphate in the surface layer (Figure 7a), maintained through export production and circulation, is similar to previous simulations with the full HAMOCC3 [e.g., *Maier-Reimer*, 1993; *Winguth et al.*, 1994] and generally reproduces the observed distribution from *Conkright et al.* [1994]. The eastern boundaries and equatorial areas of the oceans are characterized by high biological activity due to Ekman transport induced upwelling (Figure 8a) of nutrients from deeper levels and their advection in westward direction. In the subtropics, which are wideley known as biological deserts, the model reproduces the low concentrations. High phosphate concentrations are simulated in areas of low light conditions, low temperatures and high vertical mixing rates in winter time, such as the Southern Ocean. The modeled $\delta^{13}C$ distribution for the western Atlantic, which is diagnostically derived from the phosphate concentration by formula (2), is shown in Figure 9a. The simulated gradients for the modern Atlantic generally agree with observations shown in Figure 1a (adapted after

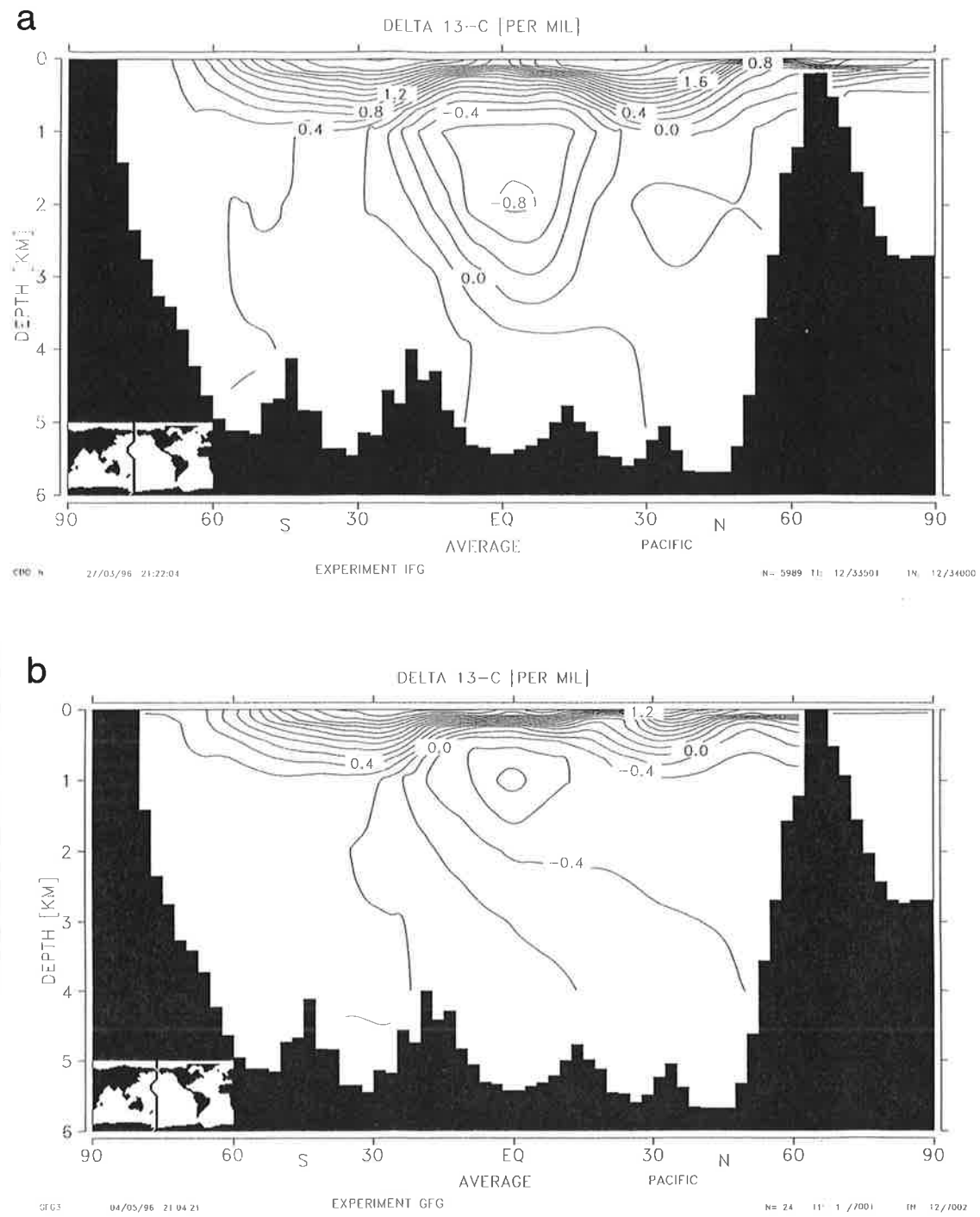

Fig. 10. Annual mean of $\delta^{13}C$ in a section of the central Pacific: (a) OGCM response to present-day boundary conditions (IFG experiment), and (b) anomaly (LGM minus present-day). Contour interval: 0.2 ‰.

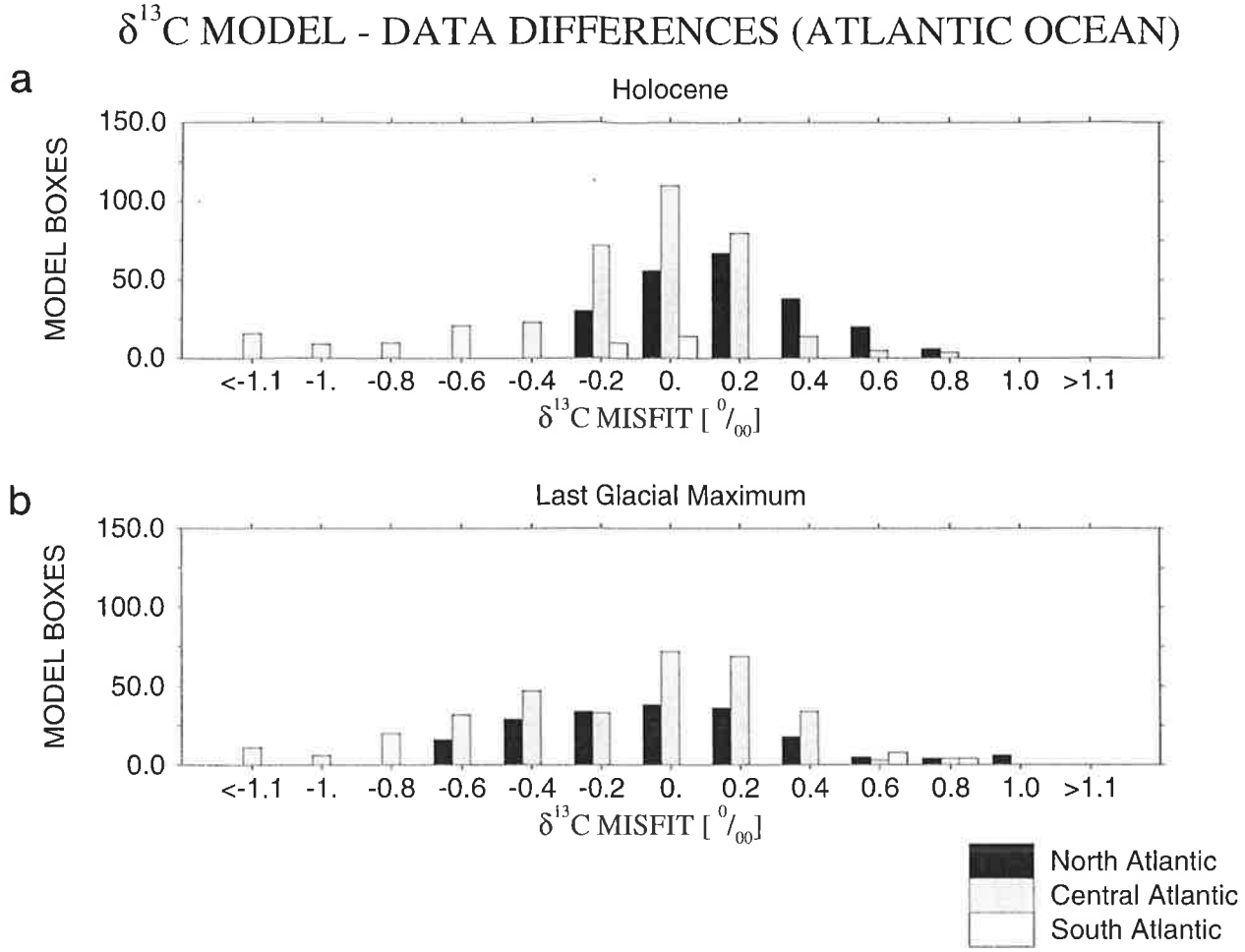

Fig. 11. Histogram of $\delta^{13}C$ misfit between the foraminifera shell $\delta^{13}C$ distribution of *Sarnthein et al.* [1994] and $\delta^{13}C$ ratios simulated by an OGCM in the northern Atlantic (black), central Atlantic (30 °N to 30 °S, grey), and the southernAtlantic (white): (a) for present-day boundary conditions (IFG experiment), and (b) for LGM boundary conditions (GFG experiment).

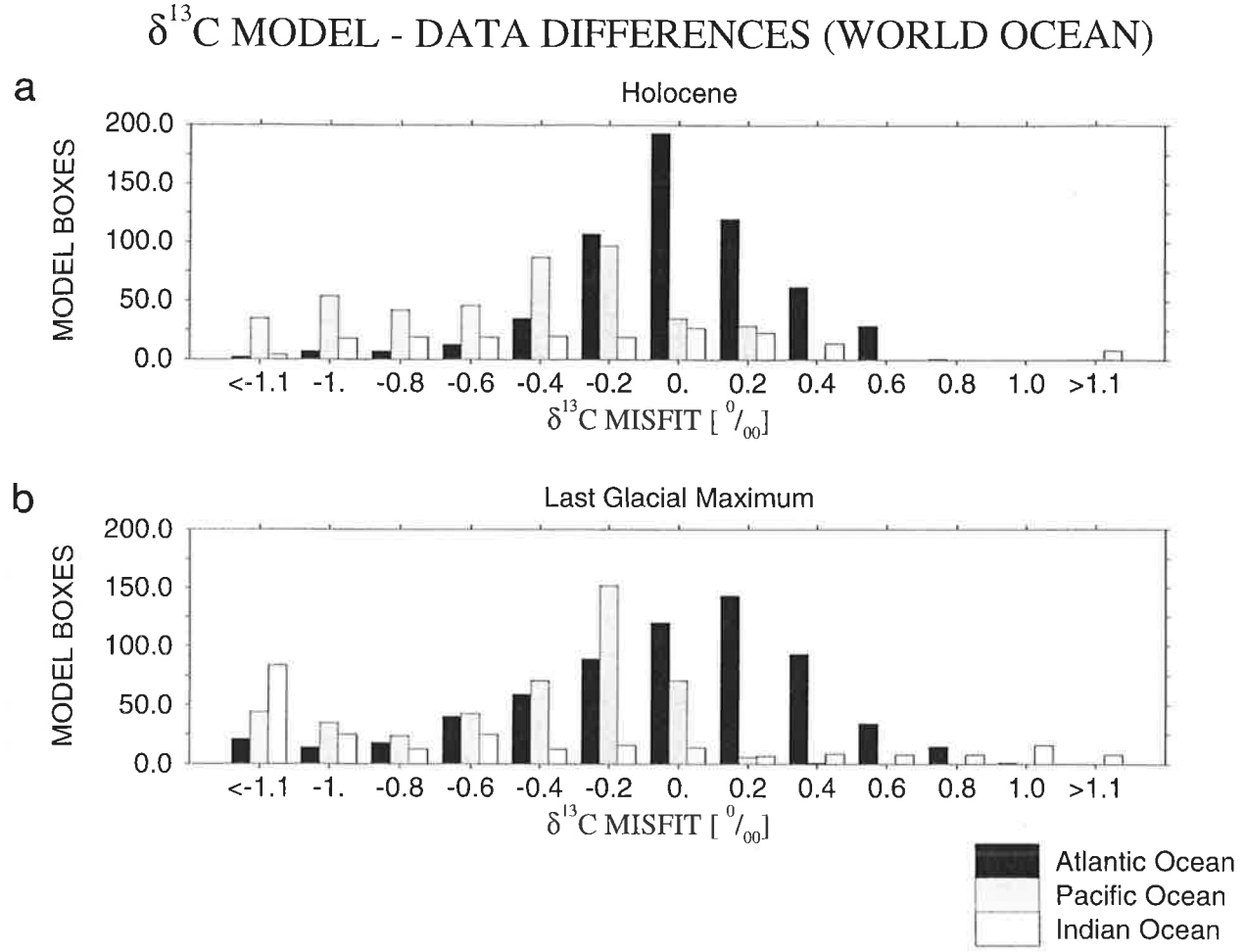

Fig. 12. Histogram of $\delta^{13}C$ misfit between the foraminifera shell $\delta^{13}C$ distribution for the deep waters of *Michel et al.* [1995] and $\delta^{13}C$ ratios simulated by our OGCM in the world ocean (Atlantic (black), Pacific (grey), and Indian Ocean (white)): (a) in response to present-day boundary conditions (IFG experiment), and (b) in response to LGM boundary conditions (GFG experiment).

Kroopnick [1985]), with high ratios in the NADW (which is young in ^{14}C age and low in nutrients). The AABW, which is comparably older in ^{14}C age and correspondingly has a higher accumulation of remineralized products, is accompanied by more negative ratios. A similar distribution of the $\delta^{13}C$ ratios in the Atlantic and Pacific (Figure 10a) has been achieved in previous studies with the 3 D carbon cycle model [*Heinze et al.*, 1991].

Figure 11a shows a histogram of disagreements between the $\delta^{13}C$ ratios from epibenthic foraminifera shells (*Cibicidoides wuellerstorfi*) in the Atlantic [*Sarnthein et al.*, 1994] and the model counterparts of the boxes in nearest vicinity to the position of the marine sediment cores. Most of the misfits have deviations in the size of the error range of the data themselves which is assumed to be 0.2 ‰ according to *LeGrand and Wunsch* [1995].

The root mean square error between the modeled $\delta^{13}C$ distribution and the data from foraminifera shells in the Atlantic [*Sarnthein et al.*, 1994] is 0.41 ‰ (Table 2), about twice the error range which can be assumed for the data themselves. Areas of a high concordance between data and modeled counterparts are assigned to the western, northern, and southern Atlantic, while high deviations occur in the tropical regions. These regions are also characterized by large differences between $\delta^{13}C$ in water samples and foraminifera shells, which reflects the complexity of the biogeochemical processes in these regions.

The misfit between the global distribution of foraminiferal $\delta^{13}C$ (Figure 7a in *Michel et al.* [1995]) and the model counterparts are shown in Figure 12a. In the Indian and Pacific Ocean the agreement between $\delta^{13}C$ data and modelled counterparts is much poorer. The differences may possibly be attributed to overestimated export production, but sparse distribution of data in central parts of these oceans also leads to large uncertainties in the $\delta^{13}C$ reconstructions themselves.

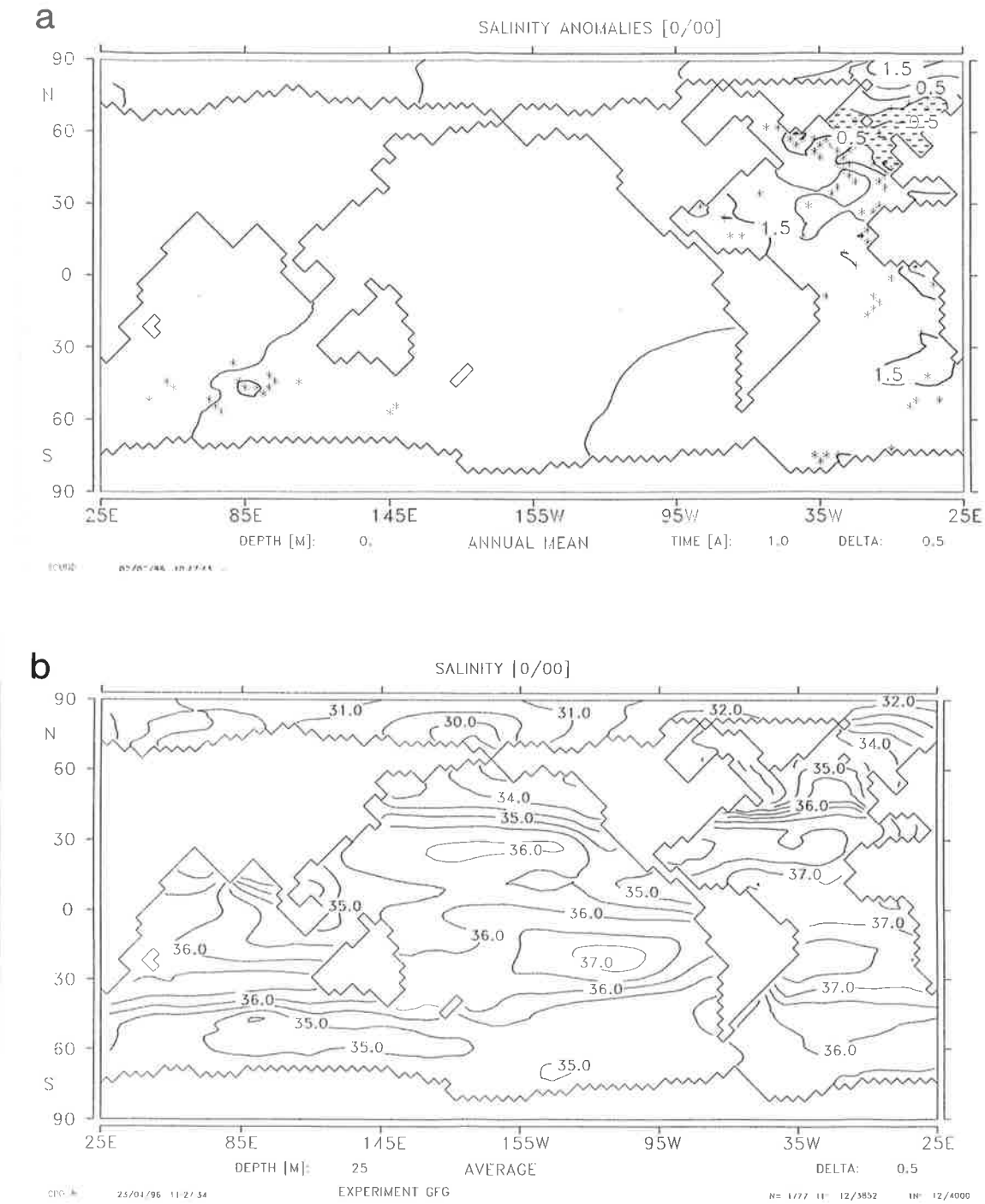

Fig. 13. (a) Reconstruction of the glacial-interglacial sea surface salinity anomalies (adapted from *Duplessy et al.* [1991], *Duplessy et al.*[manuscript in preparation] and interpolated to the model grid by advection with the 'NADW reduced' mode of *Mikolajewicz et al.* [1993]). Stars denote data locations. (b) Annual mean of surface salinty from the OGCM response to LGM boundary conditions (GFG experiment, contour interval: 0.5 psu (1 psu = 1 ‰)).

3.2. Experiment GFG - Glacial First Guess

For reconstructing a glacial circulation which is in agreement with the $\delta^{13}C$ distribution adapted from analysis of foraminifera shells [*Sarnthein et al.*, 1994; *Michel et al.*, 1995], the model was spun up with LGM boundary conditons (Table 1). Prescribed monthly mean air temperatures and wind stress were derived from the LGM experiment with the atmospheric general circulation model ECHAM3/T42 [*Lorenz et al.*, manuscript submitted], which in turn was forced with LGM sea surface temperature reconstructions from CLIMAP Project Members [1981]. The salinity surface boundary condition was obtained by adding glacial-interglacial salinity anomalies to the annual mean salinity of *Levitus* [1982]. The salinity anomalies were estimated using salinity reconstructions from the $\delta^{18}O$ ratio in planctonic foraminifera shells [*Duplessy et al.*, 1991, *Duplessy et al.*, manuscript in preparation] and include a global +1 psu [*Fairbanks*, 1989] increase due to the storage of water in the great Laurentide and Fennoscandian ice sheets. Because of the sparse distribution, the salinity values derived from the $\delta^{18}O$ data were interpolated to the model grid by advection with the 'NADW reduced' mode of *Mikolajewicz et al.* [1993](Figure 13a). This method has the feature that the interpolated fields tend to smooth the gradients of the reconstructed pattern. The model forced with this boundary condition yielded an Atlantic 'conveyor belt' even stronger than the present day one, and hence was not able to reproduce a circulation in concordance to the distribution of foraminiferal $\delta^{13}C$.

In order to drive the circulation towards a first guess of minimal $\delta^{13}C$ model-data distance, an additional anomaly had to be added to the reconstructed LGM surface salinity fields according to the 'NADW reduced' experiment of *Mikolajewicz et al.* [1993]. The salinity was modified in the Atlantic Ocean by -0.50 psu north of 50 °N and +0.75 psu south of 50 °S (including a linear transition between 40° and 50°). Nevertheless, the salinity fields of the top 50-m model layer (Figure 13b) still agree with reconstructions of *Duplessy et al.*[1991](Figure 9), with the 37 psu isohaline at 40 °N

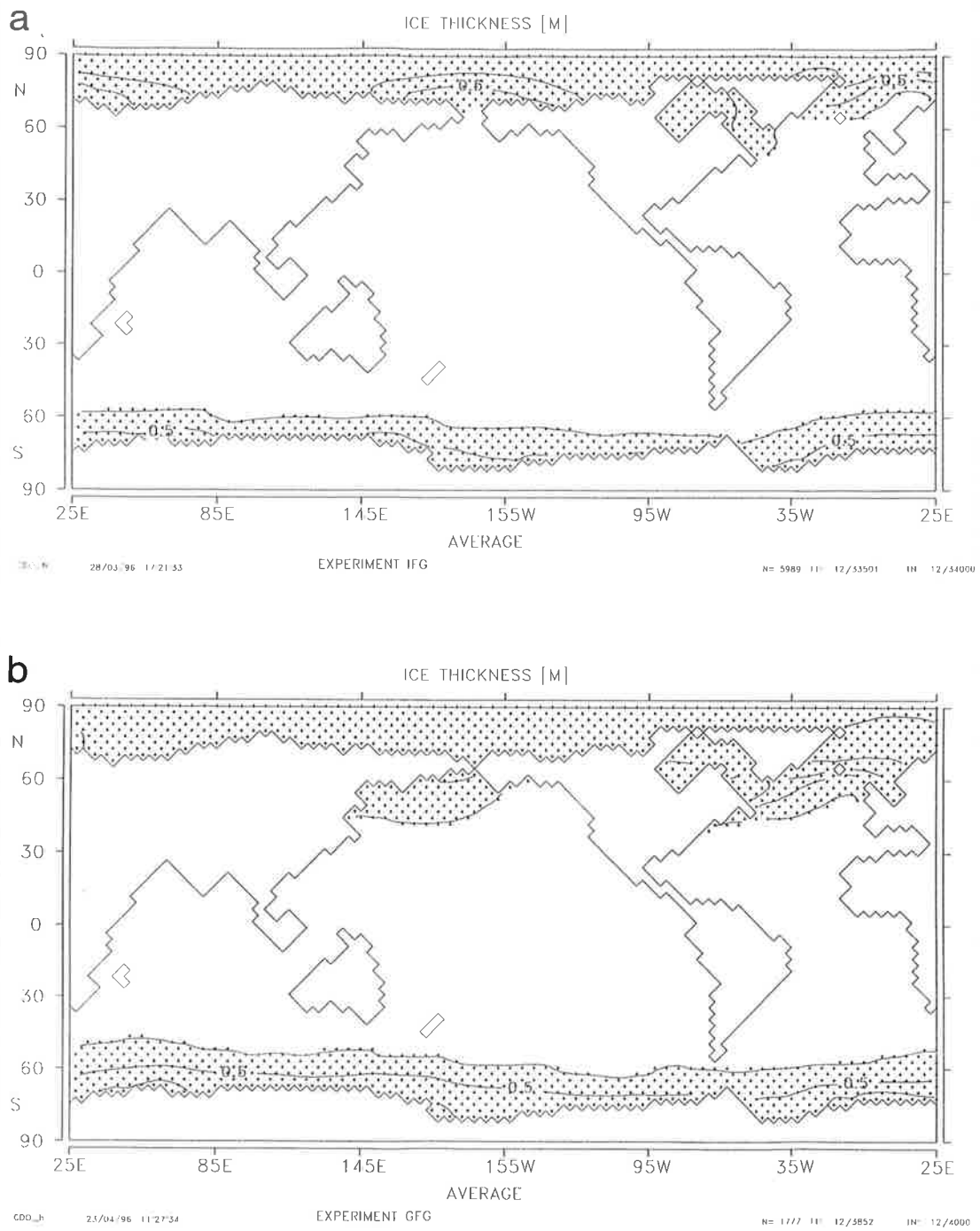

Fig. 14. Annual mean of ice thickness: (a) OGCM response to present-day boundary conditions (IFG experiment), and (b) OGCM response to LGM boundary conditions (GFG experiment). Contour interval: 0.5 m.

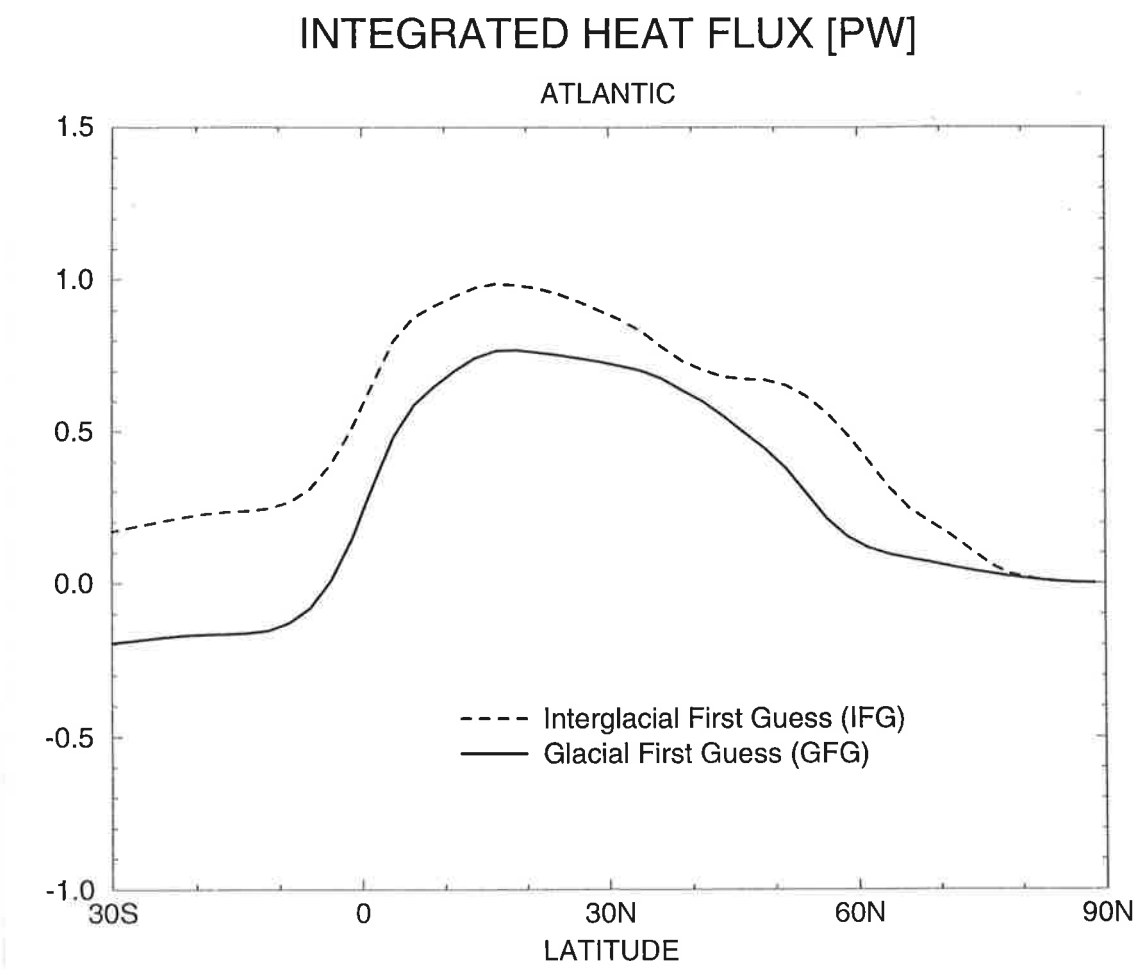

Fig. 15. Zonally integrated transport of heat: OGCM response to present-day boundary conditions (IFG experiment, dashed), and to LGM boundary conditions (GFG experiment, solid).

and the 35 psu at 60 °N south of Iceland. The distribution of sea ice (Figure 14), strongly dependent on the prescribed surface temperature, has an average ice thickness of about 2.5 m in the Arctic and extends (in the annual mean) from Newfoundland in the west to Ireland in the east. The Antarctic sea ice coverage extends up to 50 °S. It has thus, in accordance with *Cooke and Hays* [1982], approximately the double size of the Holocene sea ice extend.

Figure 2b shows the meridional circulation in the Atlantic with a reduced maximum overturning to 14 Sv at 30 °N (as compared to 11 Sv estimated by the zonally averaged model of *Fichefet et al.*[1994]) and 8 Sv at 30 °S, which is about half of the values obtained from the IFG experiment with Holocene boundary conditions. The intensification of AABW formation causes an increase of the inflow from the south into the deep Pacific (Figure 3b). The tropical Ekman cell is significantly reduced due to a weakening of the Hadley cell and negative zonal vorticity in the North Pacific.

Figure 4b shows simulated glacial-interglacial temperature anomalies with a cooling in the deep Atlantic (lower than 1500 m) from 2.6 °C to 0.6 °C in good agreement to estimates of the 2-3 °C temperature change from *Labeyrie et al.* [1987]. The deep Pacific cooled down by 0.7 °C to 1.0 °C, yielding a homogenization between deep Atlantic and deep Pacific. The meridional heat transport in the Atlantic is characterized by a reduced northward transport in the northern Hemisphere (at 30 °N reduced by roughly 20% to 0.7 PW (Figure 15)) and a southward transport in the southern Hemisphere (at 30 °S reduced by 0.3 PW). This response agrees with that simulated by *Fichefet et al.* [1994]. The vertical salinity anomalies in Figure 5b are high in the deep Southern Atlantic and tropical subsurface due to a stronger northward penetration of colder and more haline AABW. The salinity changed in the deep Atlantic by 1.29 psu to 36.30 psu and in the Pacific by 1.40 psu to 36.07 psu. Hence the salinity gradients between deep Atlantic and deep Pacific in the GFG experiment were reduced in comparison with the IFG experiment by 32%.

The simulated global mean salinity increases by 1.36 psu to 36.14 psu, i.e. 0.32 psu higher than estimations of *Duplessy et al.* [1991] which are consistent with data on sea level [*Fairbanks*, 1989]. However, the change of the global mean salinity reflects almost linearly the change of the surface boundary conditions.

We use salinities and potential temperatures of the IFG and GFG experiment to estimate rough glacial-interglacial changes in the $\delta^{18}O_{calcite}$ for the deep Atlantic and Pacific Ocean. At the LGM, $\delta^{18}O_{calcite}$ in the deep Ocean measured from benthic foraminifera shells, is in comparison with the present day ratio higher everywhere. This reflects mainly two combined effects: 1. the increased global ice volume by shifting the modern equilibrium δ^{18}O profiles by 1.-1.3 ‰ and 2. decreased water temperature. Here we use a global ice volume effect of 1.3 ‰(assuming a mean glacial-ice $\delta^{18}O_{SMOW}$ value of -42‰), consistent with data on sea level [*Fairbanks*, 1989] and a glacial-interglacial global mean salinity change of 1.36 psu. The linear relation between salinity S and $\delta^{18}O_{SMOW}$ is applied by using equation of *Zahn and Mix* [1991] for the deep sea:

$$\delta^{18}O_{SMOW\,modern} = 1.53\, S_{modern} - 53.2\,. \tag{3}$$

and

$$\delta^{18}O_{SMOW\,glacial} = 1.53\,(S_{glacial} - 1.37) - 53.2 + 1.3\,. \tag{4}$$

This yields a glacial-interglacial $\delta^{18}O_{SMOW}$ change of about 1.4 ‰ for the deep Atlantic and Pacific. To estimate the temperature effect we use the inversion of the paleotemperature equation of *Duplessy et al.* [1991]:

$$\delta^{18}O_{calcite} = \delta^{18}O_{SMOW} + 21.9 - \sqrt{310.61 + 10\,T}\,. \tag{5}$$

Thus the glacial-interglacial change of $\delta^{18}O_{calcite}$ is calculated to be 1.7 ‰ for the whole deep Atlantic in good agreement to the change derived from foraminferal analysis in the Northeast Atlantic [*Zahn and Mix*, 1991]. The simulated glacial-interglacial difference in

the deep Pacific is calculated to be 1.6 ‰, about 0.1 ‰ higher than the corresponding estimated change of *Zahn and Mix* [1991]. However, the calculations applied here are based on constant $\delta^{18}O_{SMOW}$-S slopes which possibly changed during the glacial periods.

The transport through the Drake Passage (Figure 6b) increased by 10% to about 125 Sv caused by enhanced wind stress with about the same increase in zonal direction in the Southern Ocean and stronger Antartic Bottom Water formation. This result confirms the sensitivity study of *Klinck and Smith* [1993] that the change in the wind forcing results in an almost identical change in the flow of the Antarctic Circum Polar Current. However, the 10% increase in zonal wind stress simulated by the AGCM (Figure 16) might be typically underestimated in comparison with geological evidence from sediment cores, indicating that surface winds over the the southern ocean were faster during the LGM by a factor ranging from 30% to 70% [*Klinck and Smith*, 1993]. By contrast, the transport through the Banda Street has not changed significantly. The North Atlantic subtropical gyre is intensified by the stronger glacial atmospheric west wind drift and its northern bounds shifted more southward. Thus the North Atlantic Current reaches Europe near the Bay of Biscay. A northern component of the current system along the Norwegian Coast exists as in the IFG experiment and hence transports heat in the polar region. The winddriven subtropical gyre in the northern Pacific substantially decreased by more than 10 Sv, including a reversal of the Kuroshio leading to a southward flow along the southeast Asian coast. These changes reflect the glacial-interglacial changes in the wind field caused by a possibly overestimated land/sea temperature gradient in this region. The potential uncertainties in the temperature gradients possibly reflect also problems with the accuracy of the sea surface temperature reconstructions.

We assume for phosphate for the GFG experiment a general increase in concentration of 3% due to the change of sea level of about 120 m [*Fairbanks*, 1989]. The Ekman induced upwelling in the tropical eastern Atlantic increased in comparison

with the IFG experiment by about 20% (Figure 8b), and thus this area shows high glacial phosphate concentrations (Figure 7b). In the tropical Pacific the change in the distribution behaves in the opposite way caused by weakening of the Ekman induced upwelling. The increased upwelling in the tropical Atlantic generally agrees with geological reconstructions [e.g., CLIMAP, 1981; *Sarnthein et al.*, 1988; *Yu et al.*, 1996], but simulated values in the tropical Pacific obtained here are still in contradiction to intensified glacial nutrient pattern estimated by *Farrell et al.* [1995] and a stronger glacial paleoproductivity calculated by *Peterson et al.* [1991]. However, the available $\delta^{13}C$ data in the eastern tropical Pacific do not support a dramatic change in the productivity pattern [*Michel et al.*, 1995].

We assume a glacial-interglacial global mean change of the $\delta^{13}C$ ratio of about -0.4 ‰ due to changes of land biosphere [*Crowley*, 1995]. In the Atlantic (Figure 9b) and Pacific (Figure 10b) simulated gradients of the $\delta^{13}C$ ratio generally agree with the reconstructed pattern from foraminifera shells in Figure 1b and Figure 7b in *Michel et al.* [1995]. The strongest differences occur in regions of high productivity in the deep South Atlantic and parts of Antarctic Circumpolar Current where mixing might be overestimated in the model and hence causes too high simulated $\delta^{13}C$ ratios.

Model-data differences are also displayed in Figure 11b and 12b. The best fit is obtained for the Atlantic Ocean, but very large differences occur in the Indian Ocean, especially in the Arabian Sea and Bay of Bengal, where glacial-interglacial changes are not resolved by the model. The general larger model-data disagreement for the LGM reflects an even larger uncertainty in the forcing from glacial boundary conditions (see Table 2 and below).

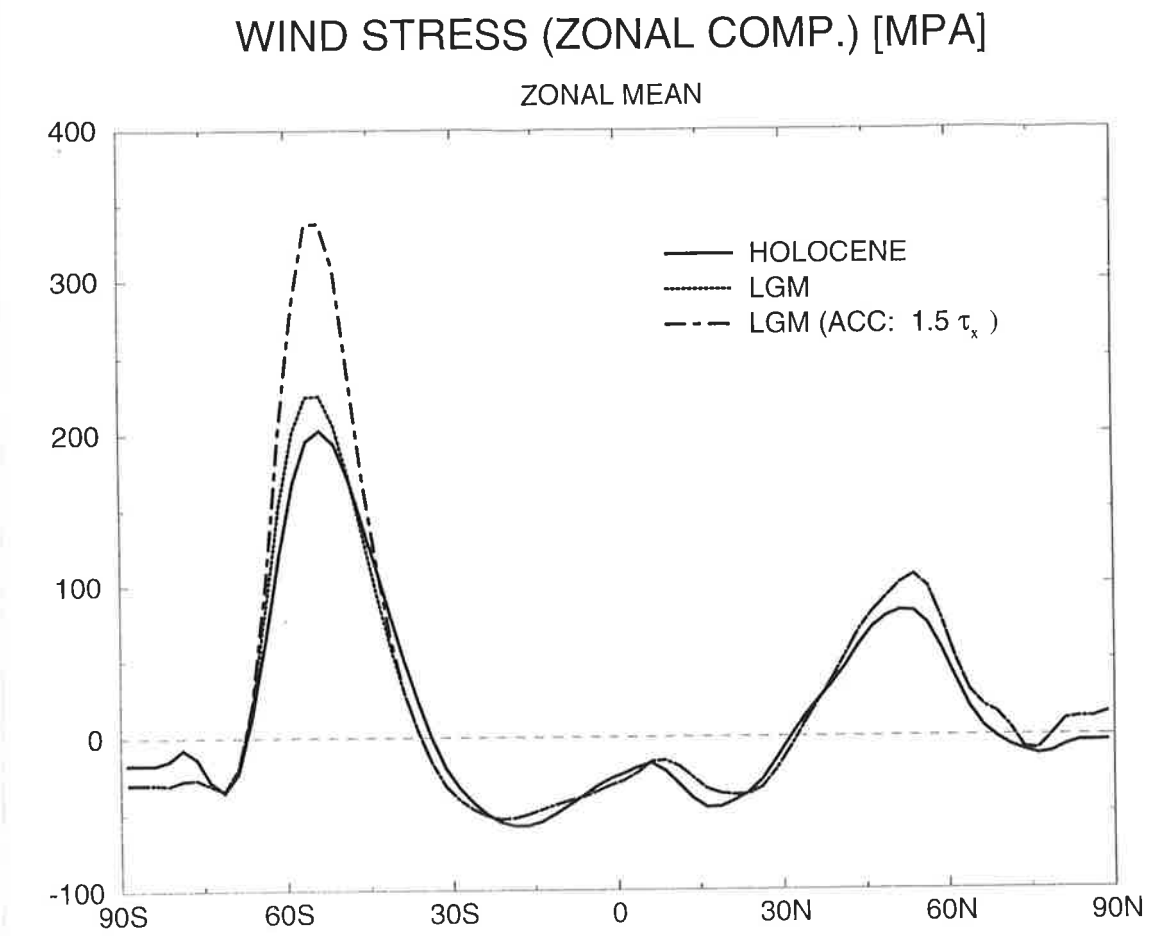

Fig. 16. Average zonal component of wind stress in response to present-day boundary conditions (solid), LGM boundary conditions (dotted), and LGM boundary conditions including an increase by a factor of 1.5 in the region between 67.5 °S and 40 °S (dot-dashed). The zonal components of wind stress were computed from experiments with the atmospheric general circulation model ECHAM3/T42.

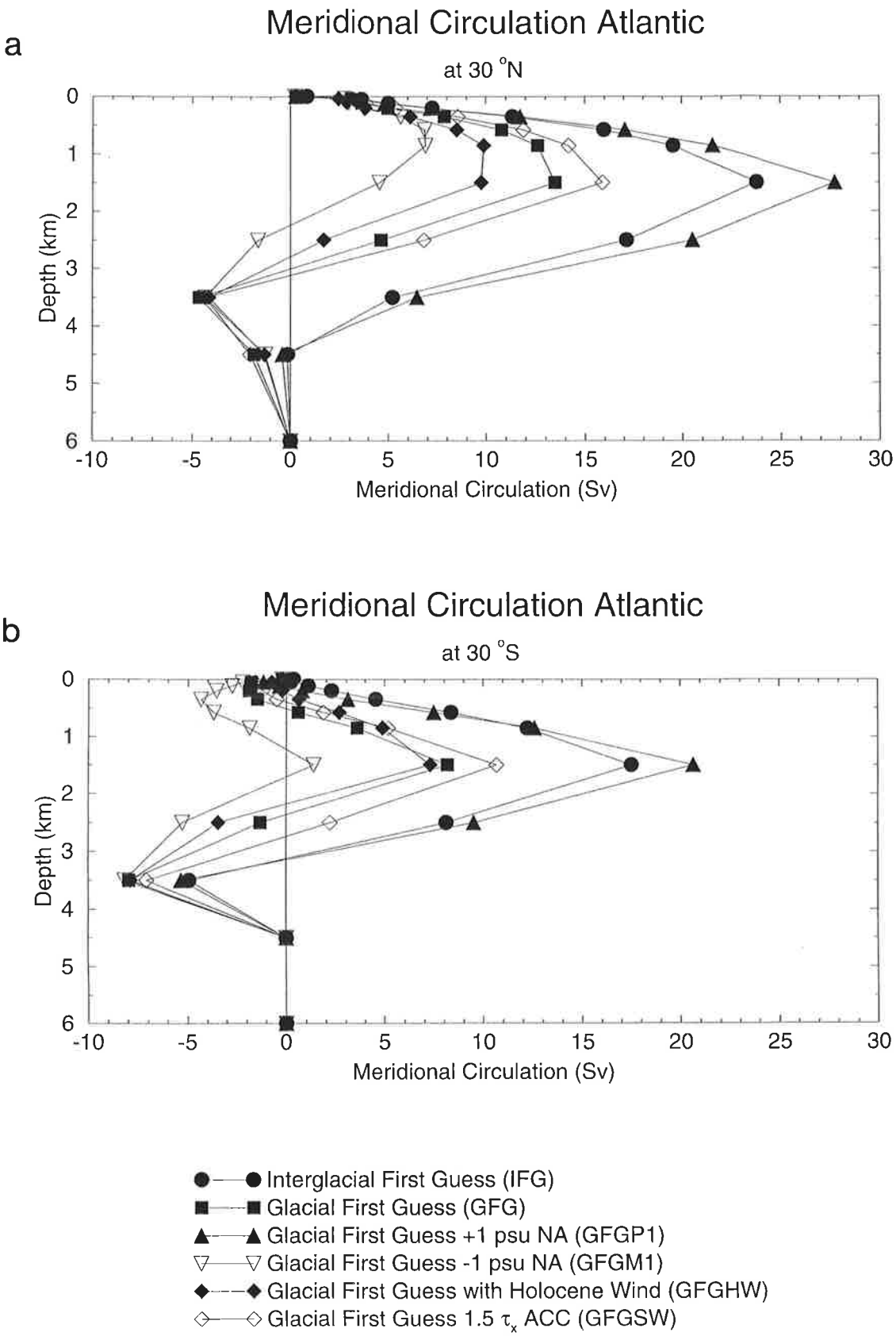

Fig. 17. Zonally integrated flow in Sverdrup (Sv) accross (a) 30 °N, and (b) 30 °S in the Atlantic for the five experiments. Positive values denote a southward flow while negative values denote a northward flow (1 Sv = 10^6 m $^3s^{-1}$).

3.3. Sensitivity to LGM salinity boundary conditions and forcing wind fields

To study the sensitivity of the thermohaline circulation due to possible errors of the reconstructed salinity boundary conditions [e.g., *Duplessy et al.*, 1991; *Fichefet et al.*, 1994; *Mikolajewicz*, 1996] two experiments have been carried out. In the two experiments GFGP1 and GFGM1 the model was forced with the same prescribed glacial boundary conditions as in experiment GFG, described in the previous section, and an additional salinity anomaly of +1 psu respectively -1 psu in the Atlantic north of 50 °N with a linear transition between 40 °N and 50 °N. Two additional experiments, GFGHW and GFGSW, were performed to investigate the sensitivity of thermohaline circulation due to uncertainties in the LGM wind fields. Both experiments used the same LGM thermohaline boundary conditions as in the GFG experiment. In experiment GFGHW we used Holocene wind stress of experiment IFG to estimate the effect of uncertainties in the range of the glacial-interglacial amplitude. In GFGSW experiment LGM wind stress was intensified in the zonal component by a factor of 1.5 in the region of the Southern Ocean (Figure 16) to consider strong glacial-interglacial wind stress changes according to *Klinck and Smith* [1993]. Figure 17 shows the Atlantic 'conveyor' at 30 °N and 30 °S of the four experiments in comparison with the interglacial and glacial first guess experiments. In GFGP1 and GFGM1 experiment a drastic change of the Atlantic 'conveyor' takes place. The change of the reconstructed salinity of +1 psu in the North Atlantic intensifies the formation of NADW and causes an even stronger circulation than the present day one under glacial boundary conditions. In GFGP1 meridional transport in the Atlantic reaches about 28 Sv at 30 °N which is about 2 times higher than the transport calculated by the GFG experiment.

By contrast, the Atlantic 'conveyor' is significantly weakend in GFGM1 by a freshening of the surface by -1 psu (a reduction by 50% of the meridional transport at 30 °N calculated from the GFG experiment). The root mean square errors between $\delta^{13}C$ data and model values of experiment GFGP1 and GFGM1 (Table 2) have higher

values than those of the GFG experiment. Experiment GFGM1 showes the best fit for south of 30 °S indicating a probably too weak simulated inflow of AABW in the GFG experiment. This sensitivity experiment also confirms the tendencies of corresponding experiments carried out with the 2 D GCM from *Fichefet et al.*[1994](Figure 3.b, page 254). Figure 17 b could be directly compared with Figure 14 in *Maier-Reimer et al.* [1993], which shows similar model behaviors by alternative formulations of the heat and fresh water boundary conditions.

Figure 17 displays also the sensitivity in respect to uncertainties in the glacial wind field. The Atlantic 'conveyor' circulation simulated by the GFGHW experiment which is driven with Holocene wind stress has almost the same feature as the circulation obtained by GFG experiment which is forced with LGM wind pattern (see also Table 2 for the deviations from the observed δ^{13}C distribution). Experiment GFGSW showes an increase of the Atlantic 'conveyor' by about 2 Sv at 30 °S and confirms similar experiments with the GFDL OGCM carried out by *Toggweiler and Samuels* [1993]. Hence misfits between modelled and observed δ^{13}C values are slightly higher as in the GFG experiment. The experiments executed here strongly support the above mentioned previous studies that the thermohaline circulation is very sensitive to changes in the bouyancy boundary conditions, while errors in the wind fields cause much smaller deviations. A realistic evaluation of uncertainties in the reconstructed surface salinity boundary conditions for the LGM therefore yields a wide spectrum of possible circulation patterns.

Table 2. Root mean square error between $\delta^{13}C$ data of *Sarnthein et al.*[1994] and $\delta^{13}C$ ratios simulated by an OGCM in the Atlantic Ocean

Latitude Belt	Experiment					
	IFG	GFG	GFGP1	GFGM1	GFGHW	GFGSW
60°- 45 °N	0.28	0.41	0.43	0.42	0.40	0.47
45°- 30 °N	0.31	0.30	0.38	0.34	0.31	0.36
30°- 15 °N	0.21	0.32	0.38	0.29	0.32	0.43
15°- 0 °N	0.52	0.51	0.50	0.64	0.49	0.52
0°- 15 °S	0.75	0.81	0.85	0.86	0.80	0.81
15°- 30 °S	0.76	0.42	0.48	0.46	0.44	0.47
30°- 45 °S	0.12	0.70	0.81	0.68	0.73	0.73
45°- 60 °S	0.12	0.57	0.68	0.50	0.59	0.58
Atlantic Ocean	0.41	0.46	0.48	0.51	0.45	0.49

4. Summary and Conclusions

We have studied the thermohaline and wind driven circulation simulated with an ocean general circulation model in response to present day and glacial prescribed boundary conditions. Generally, the model is able to reproduce the reconstructed $\delta^{13}C$ distribution from foraminifera shells. In comparison with previous attempts to simulate the glacial ocean circulation this study shows a significant reduction of the discrepancies between simulated $\delta^{13}C$ distribution and $\delta^{13}C$ ratios from foraminifera shells. However, large deviations still exist, e.g. in the area of the Antarctic Circumpolar Current and in the tropical zones of high primary productivity. These discrepancies may be due to more complex physical and biogeochemical processes in these regions.

Our model results strongly depend on the prescribed surface buoyancy boundary conditions. For example, the accuracy of the prescribed sea surface temperature from the AGCM used here reflects the accuracy of those from CLIMAP [1981]. Recent geochemical studies [*Guilderson et al.*, 1994] provide some support for the hypothesis that tropical sea surface temperatures estimated by CLIMAP are about 2-3 °C too warm. Sensitivity studies in respect to errors in the salinity boundary conditions of ± 1 psu in the North Atlantic yield circulation fields which cover the whole range from a super interglacial Atlantic 'conveyor belt' with a transport of 28 Sv to a strongly reduced transport of 7 Sv at 30 °N. A sensitivity experiment in respect to uncertainties of the wind field in range of the glacial-interglacial amplitude showed that the Atlantic overturning circulation did not change drastically. In conclusion, the results from our study support previous findings [eg. *Stocker et al.*, 1992; *Maier-Reimer et al.*, 1993; *Fichefet et al.*, 1994] that the intensity of the Atlantic 'conveyor' depends strongly upon the gradient of the high latitude buoyancy boundary conditions between the northern and southern hemispheres.

Applying optimal control techniques, such as assimilation of the $\delta^{13}C$ data from marine sediment cores into an ocean general circulation model, would provide optimal

surface boundary conditions consistent to the dynamics of the model and minimal distance between the geological data and model counterparts. Therefore, the results of this study could be used as a starting point for data assimilation.

Acknowledgments. We thank Tom Crowley, Christoph Heinze and Cornelia Winguth for fruitful discussion and carefully reading this manuscript. Also thanks to Michael Lautenschlager for several helpful comments, to Norbert Noreiks for the graphics, and to Jean-Michel Campin, Elisabeth Michel, Stefan Lorenz, and Michael Sarnthein for having provided the data used in this study. Jean-Claude Duplessy is supported by CNRS, INSU (PNEDC), and CEA. The work at the Max-Planck-Institut was supported by the Deutsche Forschungsgemeinschaft (Grant No. DFG Ma 1070/2-1).

References

Arakawa, A., and V.R. Lamb, Computational design of the basic dynamical processes of the UCLA general circulation model, *Methods Comput. Phys., 16*, 173-283, 1977.

Barnoula, J. M., D. Raynaud, Y. S. Korotkevich, and C. Lorius, Vostok ice core provides 160,000-year record of atmospheric CO_2 , *Nature, 329*, 408-414, 1987.

Berger, W.H., K. Fischer, C. Lai, and G. Wu, Ocean productivity and organic carbon flux, *SIO Ref. 87-30*, Scripps Inst. of Oceanogr., La Jolla, Calif., 1987.

Boyle, E. A., Cadmium and $\delta^{13}C$ paleochemical ocean distributions during stage 2 glacial maximum, *Annu. Rev. Earth Planet. Sci., 20*, 245-287, 1992.

Boyle, E. A., and L. D. Keigwin, North Atlantic thermohaline circulation during the past 20,000 years linked to high-latitude surface temperature, *Nature, 330*, 35-40, 1987.

Broecker, W.S., The biggest chill, *Nat. Hist. Mag., 97*, 74-82, 1987.

Broecker, W.S., An oceanographic explanation for the apprent carbon isotope-cadmium discordancy in the glacial Antarctic, *Paleoceanography, 8*, 137-139, 1993.

Broecker, W.S., and E. Maier-Reimer, The influence of air and sea exchange on the carbon isotope distribution in the sea, *Global Biogeochem. Cycles, 6*, 315-320, 1992.

Broecker, W.S., and T.-H. Peng , Carbon cycle: 1985 - Glacial to interglacial changes in the operation of the global carbon cycle, *Radiocarbon, 28*, 309-327, 1986.

Broecker, W.S., and T.-H. Peng , Interhemispheric transport of carbon dioxide by the ocean circulation, *Nature, 356*, 587-589, 1992.

CLIMAP Project Members, Seasonal reconstruction of the the earth's surface at the last glacial maximum, *Geo. Soc. Am. Map Chart Ser., MC-36*, 1981.

Conkright, M. E., S. Levitus, and T. P. Boyer, *World ocean atlas 1994: Volume 1: Nutrients*, National Oceanic and Atmospheric Administration, Washington, DC., 1994.

Cooke, D.W., and J.D. Hays, Estimates of Antarctic Ocean seasonal sea-ice cover during glacial intervals, in *Antarctic Geoscience*, edited by Craddock et al., pp. 1017-1025, Univ. Wisconsin Press, Madison, 1982.

Craig, H., and L.I. Gordon, Deuterium and oxygen-18 variations in the ocean and marine

atmosphere, in *Stable Isotopes in Oceanic Studies and Paleotemperatures*, edited by E. Tongiorgi, pp. 9-130, Consiglio Nazionale Delle Richerche, Laboratorio Di Geologia Nucleare, Pisa, 1965.

Crowley, T.J., Ice age terretrial carbon changes revisted, *Paleoceanography, 9*, 377-389, 1995.

Crowley, T.J., and G.R. North, *Paleoclimatolgy*, 339 pp., Oxford University Press, New York, 1991.

Curry, W.B., and G.P. Lohmann, Reduced advection into Atlantic deep eastern basins during last glacial maximum, *Nature, 306*, 577-580, 1983.

Dugdale, R.C., Nutrient limitation in the sea: Dynamics, identification and significance, *Limnol. Oceanogr., 12*, 685-695, 1967.

Duplessy, J. C., N.J. Shackleton, R.G. Fairbanks, L.D. Labeyrie, D. Oppo, and N. Kallel, Deep water source variations during the last climatic cycle and their impact on the global deepwater circulation, *Paleoceanography, 3*, 343-360, 1988.

Duplessy, J.C., L.D. Labeyrie, A. Juillet-Leclerc, F. Maitre, J. Dupart, and M. Sarnthein, Surface salinity reconstruction of the North Atlantic Ocean during the last glacial maximum, *Oceanologica Acta, 14*, 311-324, 1991.

England, M.H., Representing the global-scale water masses in ocean circulation models, *J. Phys. Oceanogr., 23*, 1523-155, 1993.

Eppley, R., and B.T. Peterson, Particulate organic matter flux and planktonic new production in the deep ocean, *Nature, 282*, 677-680, 1979.

Fairbanks, R. G., A 17,000 year glacio-eustatic sea level record: Influence of glacial melting rates on the Younger Dryas event and deep-ocean circulation, *Nature, 143*, 637-642, 1989.

Farrell, J.W., T.F. Pedersen, S.E. Calvert, and B. Nielsen, Glacial-interglacial changes in nutrient utilization in the equatorial Pacific Ocean, *Nature, 377*, 514-517, 1995.

Fichefet, T., S. Hovine, and J.-C. Duplessy, A model study of the Atlantic thermohaline circulation during the last glacial maximum, *Nature, 372*, 252-255, 1994.

Guilderson, T.P., R.G. Fairbanks, and J.L. Rubenstone, Tropical temperature variations since 20,000 years ago: Modulating interhemispheric climate change, *Science, 263*, 663-665,

1994.

Heinze C., and K. Hasselmann, Inverse multiparameter modelling of paleoclimatic carbon cycle indices, *Quaternary Research, 40*, 281-296, 1993.

Heinze C., E. Maier-Reimer, and K. Winn, Glacial pCO_2 reduction by the world ocean: Experiments with the Hamburg carbon cycle model, *Paleoceanography, 6*, 395-430, 1991.

Honjo, S., S.J. Manganini, and J. Cole, Sedimentation of biogenic matter in the deep ocean, *Deep Sea Research, 29*, S. 609-625, 1982.

Hughes, T.M.C., and A.J. Weaver, Multiple equilibria of an asymmetric two-basin ocean model, *J. Phys. Oceanogr., 24*, 619-637, 1994.

Keigwin, L.D., G.A. Jones, and P.N. Froehlich, A 15,000 year paleoenviromental record from Meiji Seamount, far northwest Pacific,*Earth Planet. Sci. Lett.*, 111, 425-440, 1992.

Keir, R.S., On the late Pleistocene Ocean geochemistry and circulation, *Paleoceanography, 3*, 413-446, 1988.

Klinck, J.M., and D.A. Smith, Effect of wind changes during the last glacial maximum on the circulation in the Southern Ocean, *Paleoceanography, 8*, 427-433, 1993.

Knox Ennever, F., and M.B. McElroy, Changes in atmospheric CO_2: Factors regulating the glacial to interglacial transition, in *The Carbon Cycle and Atmospheric CO_2: Natural Variations Archean to Present, Geophys. Monogr. Ser.*, vol. 32, edited by E. T. Sunquist and W. S. Broecker, pp. 154-162, AGU, Washington, D. C., 1985.

Kroopnick, P.M., The distribution of $\delta^{13}C$ of ΣCO_2 in the world oceans, *Deep Sea Res. Part A, 32*, 57-84, 1985.

Labeyrie, L.D., J.-C. Duplessy, and P.L. Blanc, Variations in mode of formation and temperature of deep waters over the past 125,000 years, *Nature, 327*, 477-482, 1987.

Labeyrie, L.D., J.C. Duplessy, J. Dupart, A. Juillet-Leclerc, J. Moyes, E. Michel, N. Kallel, and N.J. Shackleton, Changes in the vertical structure of the North Atlantic Ocean between glacial and modern times, *Quat. Sci. Rev., 11*, 401-413, 1992.

Lautenschlager, M., U. Mikolajewicz, E. Maier-Reimer, and C. Heinze, Application of ocean models for the interpretation of atmospheric general circulation model experiments on

the climate of the last glacial maximum, *Paleoceanography, 7*, 769-782, 1992.

LeDimet, F., and O. Talagrand, Variational algorithms for analysis and assimilation of meteorological observations: theoretical aspects, *Tellus, 38 A*, 97-110, 1986.

LeGrand, P., and C. Wunsch, Constraints from paleotracer data on the North Atlantic circulation during the last glacial maximum, *Paleoceanography, 10*, 1011-1045, 1995.

Levitus, S., *Climatological Atlas of the World Ocean*, Prof. Pap., 13, National Oceanic and Atmospheric Administration, Rockville, Md., 1982.

Lorenz, S., B. Grieger, P. Helbig, and K. Herterich, Investigating the sensitivity of the Atmospheric General Circulation Model ECHAM 3 to paleoclimatic boundary conditions, *Geolog. Rundschau*, (submitted).

Macdonald, A.M., Property fluxes at 30 °S and their implications for the Pacific-Indian throughflow and the global heat budget, *J. Geophys. Res., 98*(C4), 6851-6868, 1993.

Maier-Reimer, E., Geochemical cycles in an ocean general circulation model. Preindustrial tracer distributions, *Global Biogeochem. Cycles, 7*, 645-677, 1993.

Maier-Reimer, E., and K. Hasselmann, Transport and storage of CO_2 in the ocean - an inorganic ocean-circulation carbon cycle model, *Climate Dyn., 2*, 63-90, 1987.

Maier-Reimer, E., and U. Mikolajewicz, Experiments with an OGCM on the cause of the Younger Dryas, in *Oceanography 1988*, edited by A. Ayala-Castanares, W. Wooster and A. Yanel-Arancibia, pp. 87-100, UNAM Press, Mexico D.F., 1989.

Maier-Reimer, E., U. Mikolajewicz, and K. Hasselmann, Mean Circulation of the Hamburg LSG OGCM and Its Sensitivity to the Thermohaline Surface Forcing, *J. Phys. Oceanogr., 23*, 731-757, 1993.

Michel, E., L. D. Labeyrie, J. C. Duplessy, and N. Gorfi, Could deep Subanarctic convection feed the world deep basins during the last glacial maximum?, *Paleoceanography, 10*, 927-942, 1995.

Mikolajewicz, U., E. Maier-Reimer, T. J. Crowley, and K.-Y. Kim, Effect of Drake and Panamanian gateways on the circulation of an ocean model, *Paleoceanography, 8*, 409-426, 1993.

Mikolajewicz, U., A meltwater induced collapse of the 'conveyor belt' thermohaline circulation

and its influence on the distribution of $\Delta^{14}C$ and $\delta^{18}O$ in the oceans, *Report No. 189*, Max-Planck-Institut für Meteorologie, Hamburg, Germany, 1996.

Östlund, H.G., C. Craig, W.S. Broecker, and D. Spencer, *GEOSECS Atlantic, Pacific and Indian Ocean Expeditions. Shorebased Data and Graphics*, GEOSECS Atlas Series, Vol. 7, 200 pp., U.S. Goverment Printing Office, Washington D.C., 1987.

Pedersen, T.F., B. Nielsen, and M. Pickering, Timing of late quaternary productivity pulses in the Panama Basin and implications for atmospheric CO_2, *Paleoceanography, 6*, 657-677, 1991.

Rahmstorf, S., Rapid climate transitions in a coupled ocean-atmosphere model, *Nature, 372*, 82-85, 1994.

Rooth, C., Hydrology and ocean circulation, *Progr. Oceanogr., 11*, 131-149, 1982.

Sarnthein, M., K. Winn, S.J.A. Jung, J.-C. Duplessy, L. Labeyrie, H. Erlenkeuser, and G. Ganssen, Changes in east Atlantic deepwater circulation over the last 30,000 years: Eight time slice reconstructions, *Paleoceanography, 9*, 209-267, 1994.

Stommel, H., Thermohaline convection with two stable regimes flow, *Tellus, 13*, 224-230, 1961.

Schäfer-Neth, C., Modellierung der Paläoozeanographie des nördlichen Nordatlantiks zur letzten Maximalvereisung, *Berichte aus dem Sonderforschungsbereich 313, Nr. 51*, Christian-Albrechts-Universität zu Kiel, 1994.

Schiller, A., U. Mikolajewicz, and A. Voss, The Stability of the Thermohaline Circulation in a Coupled Ocean-Atmosphere General Circulation Model, *Clim. Dyn.*, (submitted).

Schmitz, W.J., On the interbasin-scale thermohaline circulation, *Rev. Geophys., 33*, 151-173, 1995.

Seidov, D., M. Sarnthein, K. Stattegger, R. Prien, and M. Weinelt, North Atlantic ocean circulation during the last glacial maximum and subsequent meltwater event - a numerical model, *J. of Geophys. Res.*, 1996, in press.

Stocker, T.F., D.G. Wright, and W.S. Broecker, The influence of high latitude surface forcing on the global thermohaline circulation, *Paleoceanography, 7*, 529-541, 1992.

Takahashi, T., W.S. Broecker, and S. Langer, Redfield ratio based on chemical data from isopycnal surfaces, *J. of Geophys. Res., 90*, S. 6907-6924, 1985.

Toggweiler, J.R., and J.L. Sarmiento, Glacial to interglacial changes in atmospheric carbon dioxide: The critical role of ocean surface water in high latitudes, in *The Carbon Cycle and Atmospheric CO_2: Natural Variations Archean to Present, Geophys. Monogr. Ser.*, vol. 32, edited by E. T. Sunquist and W. S. Broecker, pp. 163-184, AGU, Washington, D. C., 1985.

Toggweiler, J.R., and B. Samuels, Is the magnitude of the deep outflow from the Atlantic Ocean actually governed by southern hemisphere winds?, in *The Global Carbon Cycle, NATO ASI Series*, vol. I 15, edited by M. Heimann, pp. 303-331, Springer-Verlag, Berlin Heidelberg, 1993.

Tziperman, E., J.R. Toggweiler, Y. Feliks, and K. Bryan Instability of the thermohlaine circulation with respect to mixed boundary conditions: Is it really a problem for realistic models?, *J. Phys. Oceanogr., 23*, 217-232, 1994.

Volk, T., and M. I. Hoffert, Ocean carbon pumps: Analysis of relative strengths and efficiencies in ocean-driven atmospheric CO_2 changes, in *The Carbon Cycle and Atmospheric CO_2: Natural Variations Archean to Present, Geophys. Monogr. Ser.*, vol. 32, edited by E. T. Sunquist and W. S. Broecker, pp. 99-110, AGU, Washington, D. C., 1985.

Weiss, R.F., The solubility of nitrogen, oxygen and argon in water and seawater, *Deep-Sea Reserch, 17*, 721-735, 1970.

Wenk, T., and U. Siegenthaler, The high-latitude ocean as a control of atmospheric CO_2, in *The Carbon Cycle and Atmospheric CO_2: Natural Variations Archean to Present, Geophys. Monogr. Ser.*, vol. 32, edited by E. T. Sunquist and W. S. Broecker, pp. 185-194, AGU, Washington, D. C., 1985.

Whitworth, T., and R.G. Peterson, Volume transport of the Antarctic Circum Polar Current from bottom pressure measurements, *J. Phys. Oceanogr., 15*, 810-816, 1985.

Winguth, A.M.E, M. Heimann, K. D. Kurz, E. Maier-Reimer, U. Mikolajewicz, and J. Segschneider, 'El Niño-Southern Oscillation related fluctuations of the marine carbon cycle, *Global Biogeochem. Cycles, 8*, 39-63, 1994.

Woodruff, S.D., R.J. Slutz, R.L. Jenne, and P.M. Steurer, A comprehensive ocean-atmosphere data set, *Bull. Am. Meteorol. Soc., 68*, 1239-1250, 1987.

Yu, E.-F., R. Francois, and M.P. Bacon, Similar rates of modern and last-glacial ocean thermohaline circulation inferred from radiochemical data, *Nature, 379*, 689-694, 1996.

Zahn, R., and A.C. Mix, Benthic foraminiferal $\delta^{18}O$ in the ocean's temperature-salinity-density field: Constraints on ice age thermohaline circulation, *Paleoceanography, 6*, 1-20, 1991.

This manuscript was prepared with the AGU LaTeX macros v3.0.